arXiv:1410.7797v2 [cond-mat.quant-gas] 9 Jan 2015

High-temperature limit of the resonant Fermi gas

Vudtiwat Ngampruetikorn,[1] Meera M. Parish,[2] and Jesper Levinsen[3]

[1] *T.C.M. Group, Cavendish Laboratory, JJ Thomson Avenue, Cambridge, CB3 0HE, United Kingdom*
[2] *London Centre for Nanotechnology, Gordon Street, London, WC1H 0AH, United Kingdom*
[3] *Aarhus Institute of Advanced Studies, Aarhus University, DK-8000 Aarhus C, Denmark*

(Dated: January 12, 2015)

We use the virial expansion to investigate the behavior of the two-component, attractive Fermi gas in the high-temperature limit, where the system smoothly evolves from weakly attractive fermions to weakly repulsive bosonic dimers as the short-range attraction is increased. We present a new formalism for computing the virial coefficients that employs a diagrammatic approach to the grand potential and allows one to easily include an effective range R^* in the interaction. In the limit where the thermal wavelength $\lambda \ll R^*$, the calculation of the virial coefficients is perturbative even at unitarity and the system resembles a weakly interacting Bose-Fermi mixture for all scattering lengths a. By interpolating from the perturbative limits $\lambda/|a| \gg 1$ and $R^*/\lambda \gg 1$, we estimate the value of the fourth virial coefficient at unitarity for $R^* = 0$ and we find that it is close to the value obtained in recent experiments. We also derive the equations of state for the pressure, density and entropy, as well as the spectral function at high temperatures.

I. INTRODUCTION

It was long ago argued that the separate phenomena of BCS pairing of fermions, observed in conventional superconductors, and Bose-Einstein condensation (BEC) can be smoothly connected [1–3]. Such a BCS-BEC crossover may be realized by increasing the strength of attractive interactions between spin-↑ and ↓ fermions, so that the system evolves from weakly bound ↑-↓ pairs in the BCS limit to strongly bound bosonic dimers in the BEC regime. This scenario has been successfully achieved in recent experiments on ultracold atomic Fermi gases [4–9]. In the low-temperature superfluid phase, the same $U(1)$ symmetry is broken in the BCS and BEC limits, and for s-wave pairing one expects a smooth crossover between these limits without any phase transition. However, the nature of the low-energy quasiparticle excitations changes markedly as the interactions are varied and this affects the behavior of the system above the superfluid transition temperature T_c: For weak attraction, the normal state at low temperatures corresponds to a Fermi liquid, while for strong attraction, one instead obtains a weakly repulsive Bose liquid just above T_c [10]. Thus, the BCS-BEC crossover at zero temperature is associated with a crossover from fermionic to bosonic behavior in the normal state.

The different character of the two limits has been dramatically revealed in spin-imbalanced Fermi gases. At zero temperature, if one has a large difference in the spin densities n_σ, i.e., $n_\uparrow \gg n_\downarrow$, then one obtains a first-order phase transition between a Fermi-liquid phase and a superfluid phase composed of a Bose-Fermi mixture [11–13]. Moreover, in the limit of extreme imbalance where $n_\downarrow \to 0$, it was shown that the ground state of a single spin-down particle undergoes an abrupt transition from a fermionic to bosonic quasiparticle as the attraction is increased [14–17]. However, for the unpolarized case, the manner in which fermions evolve into bosons at finite temperature is not well understood, in part because of the difficulty in theoretically treating the intermediate regime of attraction between the BCS and BEC limits. Here, we elucidate the Fermi-Bose crossover of the unpolarized gas in the *high-temperature* limit, where one can perform a controlled calculation by exploiting the virial expansion.

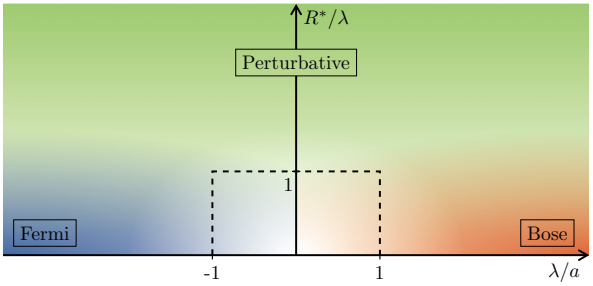

FIG. 1: Different interaction regimes for the high-temperature unpolarized Fermi gas at density $n \ll \lambda^{-3}$. When the scattering length $a < 0$ and the thermal de Broglie wavelength $\lambda \gg |a|$, the system corresponds to a weakly attractive Fermi gas. In the opposite limit, where $\lambda \gg a > 0$, the system instead resembles a weakly repulsive gas of bosonic dimers once the two-body binding energy $\varepsilon_\mathrm{b} \gg k_B T \log(\sqrt{2}/n\lambda^3)$, where T is the temperature. In the crossover region $\lambda/|a| \lesssim 1$, the system is strongly interacting in the sense that each coefficient of the virial expansion cannot be obtained from a perturbative calculation around a non-interacting system. This region can be made perturbative by introducing a large effective range parameter $R^* > \lambda$.

The high-temperature limit corresponds to a gas far from quantum degeneracy, where the thermal wavelength $\lambda \ll k_F^{-1}$, with the Fermi wavevector $k_F = (3\pi^2 n)^{1/3}$ and density $n = n_\uparrow + n_\downarrow$. Assuming short-range interactions characterized by scattering length a, the crossover in this limit is thus parametrized by the dimensionless ratio λ/a, with the system becoming a gas of bosonic dimers once λ/a is sufficiently large (Fig. 1). This is to be contrasted with the BCS-BEC crossover at zero tem-

perature, which is instead dependent on $1/k_F a$. Here, the crossover from fermionic to bosonic behavior may be defined as the point where the chemical potential μ crosses zero, since this is where BCS mean-field theory predicts a qualitative change in the quasiparticle dispersion [2, 18]. Indeed, a very recent experiment performed at temperatures $T \gtrsim T_c$ has observed the breakdown of Fermi-liquid behavior at an interaction $1/k_F a$ close to this point [19]. The low-temperature crossover is qualitatively different from its high-temperature counterpart since it is connected with the existence of a Fermi surface rather than with the thermal dissociation of dimers. However, both temperature regimes are strongly interacting near unitarity $1/a = 0$, since one cannot perform a perturbative expansion in a around a non-interacting system, unlike in the opposite limit $|a| \to 0$.

The virial or cluster expansion is one way of perturbing around a non-interacting limit for arbitrary a. In this case, the non-interacting system is the classical Boltzmann gas and the expansion parameter is the fugacity $z = e^{\beta\mu}$, where $\beta^{-1} = k_B T$ and k_B is the Boltzmann constant (which we set to 1 in the following). The coefficients of the different powers of z in the virial expansion are then functions of λ/a and determine the crossover from fermionic atoms to bosonic dimers for a given value of z. While the second order virial coefficient for short-range interactions was determined long ago [20], despite early attempts at extending the expansion – see, e.g., Ref. [21] – the extension of the virial expansion to higher powers in fugacity has only recently been achieved, mainly motivated by high precision experiments on ultracold Fermi gases. In particular, at unitarity, virial coefficients for the expansion up to z^4 have been determined both theoretically [22–25] and experimentally [26, 27]. However, the complexity of the problem increases exponentially with the order of the coefficient, and indeed it is already challenging to accurately compute the fourth virial coefficient, as exemplified by the current discrepancy between the theoretical prediction [25] and experiment [26, 27] at unitarity. For a recent review of the virial expansion as applied to the strongly interacting Fermi gas we refer the reader to Ref. [28].

One route to simplifying the calculation of the virial coefficients is to consider an interaction with an effective range, characterized by the additional length scale R^* [58]. In the limit of a "narrow resonance" $R^*/\lambda \gg 1$, we can then perform a perturbative expansion in λ/R^* for any a, as depicted in Fig. 1. This is analogous to the situation at zero temperature, where the calculation for the BCS-BEC crossover is perturbative when $k_F R^* \gg 1$ [29]. In contrast to Ref. [30], we regard the narrow-resonance case as *weakly interacting* since the limit $R^* \to \infty$ corresponds to a non-interacting mixture of fermionic atoms and bosonic dimers, as discussed below. Note that such a weakly interacting system can still exhibit a large interaction energy (e.g., at unitarity) owing to the contribution of the binding energy of the dimers.

In this paper, we present the virial expansion of the resonant Fermi gas throughout the Fermi-Bose crossover for various R^*/λ. To this end, we develop a new formalism for computing virial coefficients that employs a diagrammatic approach to the grand potential similar to that in Ref. [31], but where we use a T-matrix rather than an S-matrix description for the scattering of particles. We show that our expression for the second virial coefficient is equivalent to the well-known Beth-Uhlenbeck formula involving scattering phase shifts [20]. We also, for the first time, extend the virial expansion to higher powers of z for finite R^*. By considering the perturbative limits $\lambda/|a| \gg 1$ and $R^*/\lambda \gg 1$, we extrapolate our results and obtain an approximate value for the fourth virial coefficient at unitarity and $R^* = 0$. We also determine the equation of state in the high-temperature limit and compare with the recent MIT experiment [27].

The paper is organized as follows. In Sec. II we introduce the resonant Fermi gas as described by a two-channel model, and we discuss the role of the parameters of the model. In Sec. III we present the formalism for the virial expansion; for generality, we consider any possible spin- and mass-imbalance, any dimensionality, and any short-range model of the interactions. Section IV then concerns the virial expansion as applied to the resonant Fermi gas; we discuss the high-temperature crossover from the Fermi to Bose regime, particularly the limiting behavior of the virial coefficients, as well as how the system evolves towards a non-interacting system upon increasing the ratio of the effective range to thermal wavelength. We present exact calculations of the second and third virial coefficients, and a perturbatively exact calculation of the fourth. In Sec. V we display the high-temperature behavior of thermodynamic quantities, i.e., pressure, density, and entropy. In Sec. VI we discuss the momentum-resolved radio-frequency spectrum which one would measure in the resonant Fermi gas, focusing on the difference between broad and narrow resonances. We conclude in Sec. VII.

II. RESONANT FERMI GAS

To describe the resonant Fermi gas, we use a specific model relevant to ultracold atomic gases with short-range s-wave interactions, namely the two-channel model, introduced for bosons in Ref. [32]. This model describes how the interaction between two atoms scattering freely (in the open channel) can become resonant when they are coupled to a molecular state (closed channel) and the energy of the collision is close to that of the molecule. For the two-component Fermi gas, the Hamiltonian is

$$\hat{H} = \sum_{\mathbf{k}\sigma} \epsilon_{\mathbf{k}} \hat{c}^\dagger_{\mathbf{k}\sigma} \hat{c}_{\mathbf{k}\sigma} + \sum_{\mathbf{p}} \left(\omega_0 + \frac{p^2}{4m} \right) \hat{b}^\dagger_{\mathbf{p}} \hat{b}_{\mathbf{p}} + \frac{g}{\sqrt{V}} \sum_{\mathbf{kp}} \left(b^\dagger_{\mathbf{p}} \hat{c}_{\frac{\mathbf{p}}{2}+\mathbf{k},\uparrow} \hat{c}_{\frac{\mathbf{p}}{2}-\mathbf{k},\downarrow} + \text{h.c.} \right), \quad (1)$$

where the operator $\hat{c}^\dagger_{\mathbf{k}\sigma}$ ($\hat{c}_{\mathbf{k}\sigma}$) creates (annihilates) a fermionic atom with spin σ, momentum $\mathbf{k}$, mass m and single-particle energy $\epsilon_{\mathbf{k}} = k^2/2m$; $\hat{b}^\dagger_{\mathbf{p}}$ ($\hat{b}_{\mathbf{p}}$) creates (annihilates) a closed-channel molecule with momentum $\mathbf{p}$. g denotes the strength of the coupling which converts a pair of atoms into a closed-channel molecule — we take this to be constant up to an ultraviolet momentum cutoff Λ. ω_0 is the bare detuning, V is the volume, and we set $\hbar = 1$.

Following renormalization of the contact interaction, this Hamiltonian leads to the two-body T matrix

$$T_2(E) = \frac{4\pi/m}{a^{-1} - \sqrt{-mE} + mR^*E}, \tag{2}$$

where the bare detuning ω_0 is parameterised by the scattering length $a = (\frac{2\Lambda}{\pi} - \frac{4\pi\omega_0}{mg^2})^{-1}$ and range parameter $R^* = \frac{4\pi}{m^2 g^2}$. For positive scattering length, there exists a two-body bound state (dimer) with binding energy,

$$\varepsilon_{\rm b} = \frac{\left[\sqrt{1 + 4R^*/a} - 1\right]^2}{4mR^{*2}}. \tag{3}$$

This corresponds to a pole of the T matrix with residue

$$g^2 Z = \frac{4\pi}{m^2 R^*}\left(1 - \frac{1}{\sqrt{1 + 4R^*/a}}\right). \tag{4}$$

The gas in the resonant regime is characterized by a scattering length a which greatly exceeds the van der Waals range of the interactions, R_e, and we shall assume this to be the case in the following. Indeed, near a magnetic field Feshbach resonance, the scattering length behaves as

$$a = a_{\rm bg}\left[1 - \frac{\Delta B}{B - B_0}\right], \tag{5}$$

and can be much larger than the off-resonant background scattering length $a_{\rm bg}$ which is typically of the order of the van der Waals range. Here B is the magnetic field, while B_0 and ΔB are the location and magnetic field width of the Feshbach resonance. The effective range r_0, on the other hand, remains nearly constant across the resonance. It is typically set by the van der Waals range, but it is large and negative for Feshbach resonances which are narrow in magnetic field width such that $\mu_{\rm rel}|\Delta B| \ll 1/mR_e^2$ with $\mu_{\rm rel}$ the difference in magnetic moment of the two channels. Then it is convenient to define instead [33]

$$R^* = -r_0/2 = \frac{1}{ma_{\rm bg}\mu_{\rm rel}\Delta B}, \tag{6}$$

which relates the effective range to the experimental parameters. Thus, in the following we can use the two-body T matrix (2) to describe a realistic Feshbach resonance where the scattering length a can diverge, while the range parameter R^* is either negligible or positive.

At finite temperature, where we have thermal wavelength $\lambda = \sqrt{2\pi/mT}$, the spin- and mass-balanced Fermi gas described by the Hamiltonian (1) contains three dimensionless parameters:

$$z, \qquad \lambda/a, \qquad \lambda/R^*. \tag{7}$$

The fugacity controls the accuracy of the virial expansion, while the second parameter λ/a determines the crossover from a weakly attractive Fermi gas to a weakly repulsive Bose gas. In order to have well-defined dimers, we clearly require $\varepsilon_{\rm b} \gg T$ or equivalently $\lambda/a \gg 1$. However, entropy also plays a role at high temperature such that we always recover a Boltzmann gas of unbound atoms for sufficiently small z, i.e., for $|\mu| \gg \varepsilon_{\rm b}$. Thus, we must also consider the chemical potential (or density) of the gas when determining the regime where we have a gas of dimers. As shown in the following sections, the density in the limit $z \ll 1$ and $\varepsilon_{\rm b} \gg T$ is given by

$$n \simeq \frac{2}{\lambda^3}\left(z + 2\sqrt{2}e^{\beta\varepsilon_{\rm b}}z^2 + \ldots\right). \tag{8}$$

The second term effectively corresponds to a Boltzmann gas of dimers (where $\mu_{\rm Bose} = 2\mu + \varepsilon_{\rm b}$) while the first term is the usual Boltzmann expression for unbound atoms. Thus, we obtain the bosonic dimer regime when the second term dominates over the first, i.e., $2\sqrt{2}e^{\beta\varepsilon_{\rm b}}z \gg 1$. This yields the condition $n\lambda^3 \gg \sqrt{2}e^{-\beta\varepsilon_{\rm b}}$, which is equivalent to the expression in the caption of Fig. 1. Note, further, that when the majority of particles are bound into dimers, one obtains $\mu \lesssim -\varepsilon_{\rm b}/2$. Thus, $z \ll 1$ always, which naively suggests that the virial expansion holds all the way down to $T = 0$. However, this instead means that we must modify the virial expansion to reflect the change in quasiparticles so that the relevant expansion parameter is now $z^* = e^{\beta\varepsilon_{\rm b}/2}z$ — see also Ref. [31] and Sec. IV.

The third dimensionless parameter, λ/R^*, in turn, allows a perturbative expansion in small λ/R^* of the virial coefficients themselves. This is a consequence of the typical collision energies, set by the temperature, greatly exceeding the interaction energy scale $\sim g^4 \propto 1/R^{*2}$, rendering the system effectively perturbative in the bare coupling constant. This behavior mimics that of the many-body problem at zero temperature, which is perturbative for all scattering lengths if R^* greatly exceeds the average interparticle spacing [29]. Indeed, in that work a narrow Feshbach resonance was defined as one fulfilling $k_F R^* \gg 1$, and here we extend this definition to mean any resonant Fermi gas for which the typical interaction energies greatly exceed that set by the bare coupling. Thus, in the high-temperature limit of the resonant Fermi gas, the broad (narrow) resonance limits correspond to $\lambda/R^* \gg 1$ ($\lambda/R^* \ll 1$), respectively.

III. VIRIAL EXPANSION

We now present the virial expansion of the grand potential for a two-component ($\uparrow$, $\downarrow$) Fermi system with

contact interspecies interaction. For the sake of generality, we do not restrict ourselves to a system described by the Hamiltonian (1); instead we consider the problem in d dimensions and for arbitrary mass ratio $m_\uparrow/m_\downarrow$. We note that the formalism outlined in this section may be straightforwardly extended to more fermionic components, a Bose gas, or even a Bose-Fermi mixture. In Sec. IV we apply the results of the present section to the resonant Fermi gas described by the two-channel Hamiltonian (1).

For a Hamiltonian $\hat{H}$, the grand potential is given by (see, e.g., [34])

$$\begin{aligned} -\beta\Omega &= \sum_{\{N_\sigma\}} \left[\mathrm{Tr}_{\{N_\sigma\}}\, \hat{A} e^{-\beta(\hat{H}-\sum_\sigma \mu_\sigma \hat{N}_\sigma)}\right]_c \\ &= \sum_{N_\uparrow N_\downarrow} z_\uparrow^{N_\uparrow} z_\downarrow^{N_\downarrow} \left[\mathrm{Tr}_{N_\uparrow N_\downarrow}\, \hat{A} e^{-\beta\hat{H}}\right]_c, \end{aligned} \tag{9}$$

where $\hat{N}_\sigma$ is the number operator of σ particles, μ_σ is the chemical potential for each spin, and $z_\sigma = e^{\beta\mu_\sigma}$. The suffix c indicates that only connected diagrams are kept and the operator $\hat{A}$ represents the sum of all identical particle permutations with negative signs affixed in front of odd permutations: $\hat{A} \equiv \sum_P (-1)^P P$ where P is a permutation acting only among identical particles, with $(-1)^P$ the sign of the permutation. The sum over non-negative N_σ is such that the total number of particles $\sum_\sigma N_\sigma$ is positive. The trace on states of the system is taken at fixed particle number. When the temperature is high or the system dilute, the thermodynamics of the system can be accurately described by the first few terms of the above power series. That is, the thermodynamics is essentially determined by few-body physics. However, to establish such a connection, it is convenient to separate the dynamical (microscopic) and statistical information [31].

As a starting point, we define the Green's operators (see also Ref. [31])

$$\hat{G}(E) = \frac{1}{E-\hat{H}}, \quad \hat{G}_0(E) = \frac{1}{E-\hat{H}_0}, \tag{10}$$

such that

$$e^{-\beta\hat{H}} = \oint \frac{dE}{2\pi i} e^{-\beta E} \hat{G}(E). \tag{11}$$

This formulation exactly achieves the goal of separating the statistical information from the dynamical, since $\hat{G}$ does not depend on temperature. Here, the Hamiltonian $\hat{H} = \hat{H}_0 + \hat{H}_{\mathrm{int}}$ consists of the non-interacting part $\hat{H}_0$ and the interactions $\hat{H}_{\mathrm{int}}$. E is a complex variable and the counterclockwise contour encloses the structure of the Green's operator on the real axis, i.e., the integral picks out the spectrum of $\hat{H}$. [We let $\oint$ denote a counterclockwise contour throughout this work.] For brevity, we define the linear operator

$$\oint_E' \equiv \oint \frac{dE}{2\pi i} e^{-\beta E}, \tag{12}$$

such that Eq. (11) reads

$$e^{-\beta\hat{H}} = \oint_E' \hat{G}(E). \tag{13}$$

The operator $\oint_E'$ is the Laplace transform which connects the few-body dynamics to the statistical physics. Substituting Eq. (13) in Eq. (9), we obtain

$$-\beta\Omega = \sum_{N_\uparrow N_\downarrow} z_\uparrow^{N_\uparrow} z_\downarrow^{N_\downarrow} \oint_E' \left[\mathrm{Tr}_{N_\uparrow N_\downarrow}\, \hat{A}\hat{G}(E)\right]_c. \tag{14}$$

Physically, the imaginary part of $[\ldots]_c$ on the real axis ($\Im E \to 0^+$) is the spectral density of the few-body system and the contour integral with a Boltzmann factor is therefore equivalent to counting all accessible states in the system.

Note that one must be careful when dealing with processes which contain identical subclusters: If a diagram has M distinct sub-clusters, the i'th of these appearing c_i times, then a factor of $(c_1! c_2! \cdots c_M!)^{-1}$ must be introduced when applying $\hat{A}$ to avoid double counting. This will become clear when we consider the non-interacting contributions in Section III A.

We define the virial coefficients, $B_{N_\uparrow N_\downarrow}$, such that

$$-\beta\Omega = \frac{V}{\lambda_r^d} \sum_{N_\uparrow N_\downarrow} B_{N_\uparrow N_\downarrow} z_\uparrow^{N_\uparrow} z_\downarrow^{N_\downarrow}. \tag{15}$$

where the 'reduced' thermal wavelength is given by $\lambda_r \equiv \sqrt{\pi/m_r T}$, with the reduced mass $m_r^{-1} = m_\uparrow^{-1} + m_\downarrow^{-1}$. From Eqs. (14) and (15) we identify

$$B_{N_\uparrow N_\downarrow} = \frac{\lambda_r^d}{V} \oint_E' \left[\mathrm{Tr}_{N_\uparrow N_\downarrow}\, \hat{A}\hat{G}(E)\right]_c. \tag{16}$$

The indices $N_\uparrow$ and $N_\downarrow$ indicate the number of $\uparrow, \downarrow$ particles in the connected few-body cluster and therefore $B_{N_\uparrow 0}$ and $B_{0 N_\downarrow}$ correspond to the ideal-gas contributions from $\uparrow$ and $\downarrow$ species, respectively. If both $N_\uparrow$ and $N_\downarrow$ are finite, $B_{N_\uparrow N_\downarrow}$ is non-zero only when the interspecies interaction is present.

In the particular case of a spin- and mass-balanced Fermi gas, i.e., $m \equiv m_\sigma$, $\mu \equiv \mu_\sigma$, $z \equiv z_\sigma$ with $\sigma = \uparrow, \downarrow$, Eq. (15) reduces to

$$-\beta\Omega = \frac{2V}{\lambda^d} \sum_{N \geq 1} b_N z^N, \tag{17}$$

where the thermal wavelength takes its usual form: $\lambda = \lambda_r = \sqrt{2\pi/mT}$. The virial coefficients in this case are related to those occuring in Eq. (15) above by $2b_N = \sum_{N'=0}^{N} B_{N', N-N'}$. In addition, one may separate out the effects of interaction, i.e., $b_N = b_N^{\mathrm{free}} + \Delta b_N$. The ideal-gas contribution is given by $2b_N^{\mathrm{free}} = B_{N0} + B_{0N}$ and the effect of interactions are contained in $2\Delta b_N = \sum_{N'=1}^{N-1} B_{N', N-N'}$. We note further that in a mass-balanced system, $B_{NN'} = B_{N'N}$.

It is straightforward to connect the virial coefficients for the uniform system in Eq. (17) to those for a gas confined in an isotropic harmonic trap $V(\mathbf{r}) = \frac{1}{2}m\omega^2 r^2$, where ω is the trapping frequency. Assuming we are in the limit where $\beta\omega \ll 1$, the grand potential in the trap is given by $-\beta\Omega_{\rm trap} = 2(\beta\omega)^{-d}\sum_{N\geq 1} b_N^{\rm trap} z^N$. Applying the local density approximation to Eq. (17) and comparing expressions then simply yields $b_N = N^{d/2}\, b_N^{\rm trap}$. This procedure may be easily extended to the case where m_σ, μ_σ and/or the trapping frequencies for each spin are all different.

A. $\mathbf{N_\downarrow = 0}$

In this section, we consider the ideal Fermi gas contribution to the grand potential. For $N_\uparrow = 1$ and $N_\downarrow = 0$ the Green's operator is simply

$$\hat{G}(E) = \text{——}, \tag{18}$$

where the straight line denotes the one-particle propagator. Taking the trace then requires the state on the left and right to be the same, i.e.,

$$\mathrm{Tr}_{10}\, \hat{A}\hat{G}(E) = \ 1\text{——}1 \tag{19}$$

where the repeated index indicates that the end-points have been contracted. Thus we write down the virial coefficient

$$B_{10} = \frac{\lambda_r^d}{V}\oint_E{}' \sum_{\mathbf{p}} (E - \epsilon_{\mathbf{p}\uparrow})^{-1} = \left(\frac{m_\uparrow}{2m_r}\right)^{\frac{3}{2}}. \tag{20}$$

Here and in the following the trace is evaluated in momentum states, with the single-particle energy $\epsilon_{\mathbf{p}\sigma} = p^2/2m_\sigma$.

Next we let $N_\uparrow = 2$ and write down the Green's operator

$$\hat{G}(E) = \text{——}\!\!\text{——}. \tag{21}$$

Since there is no intraspecies interaction, each particle can only propagate as a free particle. Thus, few- and many-body correlations can only arise through exchange of identical particles. Applying the exchange operator and taking the trace, we obtain

$$\mathrm{Tr}_{20}\, \hat{A}\hat{G}(E) = \frac{1}{2!}\left(\begin{smallmatrix}1\text{——}1\\2\text{——}2\end{smallmatrix} - \begin{smallmatrix}1\text{——}2\\2\text{——}1\end{smallmatrix}\right). \tag{22}$$

The factor 1/2! accounts for the fact that there are two identical clusters (one-particle propagators) in the operator $\hat{G}$. We see that the two propagators in the first term are not connected and thus only the second term contributes to the virial coefficient

$$B_{20} = \frac{\lambda_r^d}{V}\oint_E{}' \sum_{\mathbf{p}} \frac{-1}{2!}(E - 2\epsilon_{\mathbf{p}\uparrow})^{-1} = \left(\frac{m_\uparrow}{2m_r}\right)^{\frac{3}{2}} \frac{-1}{2\cdot 2^{\frac{d}{2}}},$$

Note that the consequence of the trace is that each particle carries the same momentum.

For $N_\uparrow = 3$, there are 3! permutations, two of which are connected; hence,

$$[\mathrm{Tr}_{30}\, \hat{A}\hat{G}(E)]_c = \frac{1}{3!}\left(\begin{smallmatrix}1\text{——}3\\2\text{——}1\\3\text{——}2\end{smallmatrix} + \begin{smallmatrix}1\text{——}2\\2\text{——}3\\3\text{——}1\end{smallmatrix}\right) = \frac{2}{3!}\cdot \begin{smallmatrix}1\text{——}3\\2\text{——}1\\3\text{——}2\end{smallmatrix}$$

This leads to

$$B_{30} = \frac{\lambda_r^d}{V}\oint_E{}' \sum_{\mathbf{p}} \frac{2}{3!}(E - 3\epsilon_{\mathbf{p}\uparrow})^{-1} = \left(\frac{m_\uparrow}{2m_r}\right)^{\frac{3}{2}} \frac{1}{3\cdot 3^{\frac{d}{2}}}.$$

It is easy to verify that for any $N_\uparrow > 0$, there are $(N_\uparrow - 1)!$ connected diagrams each with identical contribution and permutation sign $(-1)^{N_\uparrow - 1}$. Hence, the virial coefficients of a free Fermi gas are given by

$$B_{N_\uparrow 0} = \left(\frac{m_\uparrow}{2m_r}\right)^{\frac{3}{2}} \frac{(-1)^{N_\uparrow - 1}}{N_\uparrow \cdot N_\uparrow^{\frac{d}{2}}}. \tag{23}$$

In a spin- and mass-balanced Fermi gas, Eq. (23) yields $b_N^{\rm free} = \frac{1}{2}(B_{N0} + B_{0N}) = \frac{(-1)^{N-1}}{N\cdot N^{d/2}}$, as expected.

B. $\mathbf{N_\uparrow = N_\downarrow = 1}$

In order to deal with interactions, we use the fact that the full Green's operator can be written in terms of the free Green's operator and the T matrix, defined such that $\hat{T}^{-1}(E) = \hat{H}_{\rm int}^{-1} - \hat{G}_0(E)$. For the case of $N_\uparrow = N_\downarrow = 1$, we write down the Green's operator

$$\hat{G}(E) = \hat{G}_0(E) + \hat{G}_0(E)\hat{T}_2(E)\hat{G}_0(E) = \text{——} + \text{>···<}, \tag{24}$$

where ····· denotes the two-body T operator $\hat{T}_2(E)$ and particles of different species are depicted by different colours. Then, the trace of $\hat{G}$ is given by

$$\mathrm{Tr}_{11}\, \hat{G}(E) = \begin{smallmatrix}1\text{——}1\\1\text{——}1\end{smallmatrix} + \begin{smallmatrix}1\\1\end{smallmatrix}\text{>···<}\begin{smallmatrix}1\\1\end{smallmatrix}. \tag{25}$$

Since the two particles are distinguishable there are no additional exchange terms. Discarding the disconnected diagram, one obtains

$$[\mathrm{Tr}_{11}\, \hat{G}(E)]_c = \begin{smallmatrix}1\\1\end{smallmatrix}\text{>···<}\begin{smallmatrix}1\\1\end{smallmatrix} = \mathrm{Tr}_{11}\, \hat{G}_0(E)\hat{T}_2(E)\hat{G}_0(E) \tag{26}$$

$$= \mathrm{Tr}_{11}\, \hat{T}_2(E)\frac{d}{dE}\hat{T}_2^{-1}(E), \tag{27}$$

where in the last step we used the cyclic property of the trace and the identity: $\frac{d}{dE}\hat{T}^{-1}(E) = -\frac{d}{dE}\hat{G}_0(E) = \hat{G}_0^2(E)$.

The two-body T matrix is given by

$$\hat{T}_2(E) = \sum_{\mathbf{P}}\sum_{\ell,\ell_z} T_{2,\ell}(E - P^2/2M)\,|\mathbf{P},\ell\rangle\langle\mathbf{P},\ell|\,, \tag{28}$$

where $\mathbf{P}$ denotes the centre-of-mass momentum, ℓ (ℓ_z) the total (magnetic) angular momentum quantum number and $M = m_\uparrow + m_\downarrow$ is the total mass. The T matrix is independent of the magnetic quantum number, resulting in the degeneracy factor $\xi_\ell \equiv \sum_{\ell_z}$: This takes the value $2\ell+1$ in 3D, $2-\delta_{0,\ell}$ in 2D, and 1 in 1D (where ℓ is restricted to 0 or 1). Both $\mathbf{P}$ and ℓ are conserved quantities and thus $\hat{T}_2$ is diagonal in this representation. The inverse of this operator is thus given by

$$\hat{T}_2^{-1}(E) = \sum_{\mathbf{P},\ell} \xi_\ell T_{2,\ell}^{-1}(E - P^2/2M)\,|\mathbf{P},\ell\rangle\langle\mathbf{P},\ell|\,. \quad (29)$$

As a result, Eq. (27) reads

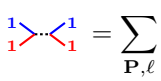
$$= \sum_{\mathbf{P},\ell} \xi_\ell T_{2,\ell}\left(E - \frac{P^2}{2M}\right) \frac{d}{dE} T_{2,\ell}^{-1}\left(E - \frac{P^2}{2M}\right). \quad (30)$$

Hence, the second virial coefficient is given by

$$B_{11} = \left(\frac{M}{2m_r}\right)^{\frac{d}{2}} \oint_E{}' \sum_\ell \xi_\ell T_{2,\ell}(E) \frac{d}{dE} T_{2,\ell}^{-1}(E), \quad (31)$$

which is identical to that obtained in Ref. [24]. The prefactor results from integrating out the centre-of-mass motion, i.e., $(\lambda_r^3/V)\sum_{\mathbf{P}} \exp[-\beta \frac{P^2}{2M}] = (\frac{M}{2m_r})^{3/2}$.

The second virial coefficient (31) can be shown to be equivalent to the well-known Beth-Uhlenbeck formula. To see this, we consider the contributions from the bound states and the scattering states separately. The former is easy to extract. Near an energy pole $E = -\varepsilon_\mathrm{b}$, the T matrix is proportional to $(E+\varepsilon_\mathrm{b})^{-1}$ and thus $T_{2,\ell}(E)\frac{d}{dE}T_{2,\ell}^{-1}(E) \to (E+\varepsilon_\mathrm{b})^{-1}$. As a result, the contour integral picks up this simple pole to give

$$B_{11}^{\mathrm{poles}} = \left(\frac{M}{2m_r}\right)^{\frac{d}{2}} \sum_\mathrm{b} e^{\beta\varepsilon_\mathrm{b}},$$

where the sum is over all bound states – even if these are degenerate, they should be counted separately. To tackle the scattering states, we deform the contour to the real axis, yielding (mass ratio factor and partial-wave sum omitted)

$$-\int_0^\infty \frac{dE}{\pi} e^{-\beta E} \Im\left[\frac{d}{dE} \ln T_{2,\ell}^{-1}(E+i0)\right].$$

Noting that $T_{2,\ell}(E+i0) \propto (k\cot\delta_\ell(k) - ik)^{-1}$ with $k = \sqrt{2m_r E}$, the integral above reduces to

$$\int_0^\infty \frac{dE}{\pi} e^{-\beta E} \frac{dk}{dE} \delta_\ell'(k).$$

Replacing E with $k^2/2m_r$, we recover the Beth-Uhlenbeck formula (see, e.g., [35])

$$B_{11} = \left(\frac{M}{2m_r}\right)^{\frac{d}{2}} \left[\sum_\mathrm{b} e^{\beta\varepsilon_\mathrm{b}} + \sum_\ell \xi_\ell \int_0^\infty \frac{dk}{\pi} e^{-\frac{\beta k^2}{2m_r}} \delta_\ell'(k)\right]. \quad (32)$$

Finally, we note that in the spin- and mass-balanced system, the part of the virial coefficient arising from interactions is obtained from the relation $2\Delta b_2 = B_{11}$.

C. $\mathbf{N_\uparrow = 2}$; $\mathbf{N_\downarrow = 1}$

In this section, we consider the contribution to the grand potential from the few-body cluster with two $\uparrow$ and one $\downarrow$ atoms. In this case the Green's operator reads

$$\hat{G}(E) = \quad (33)$$

We see that the first diagram corresponds to free propagation and is disconnected. The second term appears, at first glance, to be disconnected but we shall see that the one-particle and two-particle sub-clusters can be connected via exchange. Since the largest sub-cluster in the second term contains two particles, we will call this term the 'two-body' contribution. The remaining terms are fully connected and thus we refer to these collectively as the 'three-body' contributions.

In the next step, we apply the permutation operator and take the trace. After discarding the free propagator, we have

$[\mathrm{Tr}_{21}\,\hat{A}\hat{G}(E)]_\mathrm{int} =$

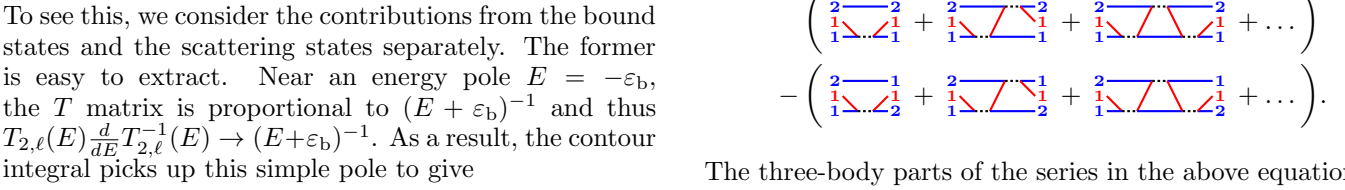

The three-body parts of the series in the above equation may be replaced by three-body propagators, but first it is instructive to reorganize the diagrams into two groups: (i) diagrams where the T_2's on the left and right are labelled by the same indices and (ii) those where they are labelled by different indices. Following the reorganization, the two sets of diagrams are

$[\mathrm{Tr}_{21}\,\hat{A}\hat{G}(E)]_\mathrm{int} =$

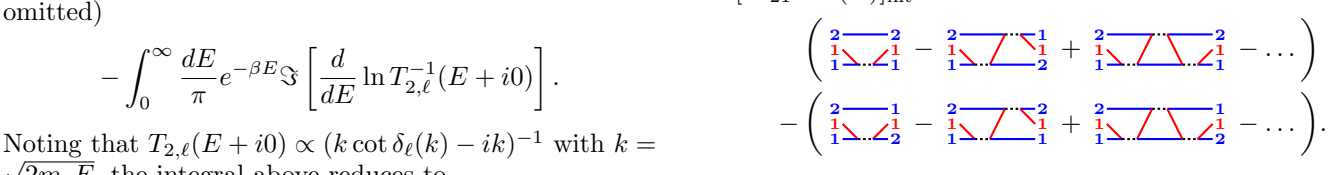

It is clear that the left-most term in the first set is disconnected and therefore does not contribute to the virial coefficient.

We then define the three-body T matrix t_3:

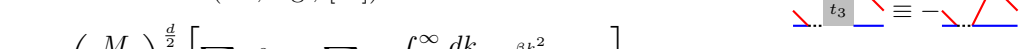
$$\equiv \quad (34)$$

where t_3 can be obtained from solving the Skorniakov–Ter-Martirosian integral equation [36], properly generalized to the present problem. For details, see Appendix

A. Hence, the virial coefficient reads

$$B_{21} = \frac{\lambda_r^d}{V}\oint_E' \Big(\quad - \quad - \quad \Big)$$

$$= \left(\frac{M_{21}}{2m_r}\right)^{\frac{d}{2}} \oint_E' \sum_{\mathbf{p}} \Bigg[\chi_{21}(\mathbf{p},\mathbf{p};E) \frac{dT_2^{-1}\left(E-\frac{p^2}{2m_{21}}\right)}{dE} - \frac{T_2(E-p^2/2m_{21})}{\left(E-2\epsilon_{\mathbf{p}\uparrow}-\epsilon_{2\mathbf{p}\downarrow}\right)^2} - \sum_{\mathbf{p}'} \frac{\chi_{21}(\mathbf{p},\mathbf{p}';E)}{\left(E-\epsilon_{\mathbf{p}\uparrow}-\epsilon_{\mathbf{p}'\uparrow}-\epsilon_{\mathbf{p}+\mathbf{p}'\downarrow}\right)^2} \Bigg], \quad (35)$$

with $\chi_{21}(\mathbf{p},\mathbf{p}';E) \equiv T_2(E-\frac{p^2}{2m_{21}})t_3^{\uparrow\uparrow\downarrow}(\mathbf{p},\mathbf{p}';E)T_2(E-\frac{p'^2}{2m_{21}})$. In the last step, the centre-of-mass motion is integrated out, giving the factor $(\frac{M_{21}}{2m_r})^{\frac{d}{2}}$. Here, the total mass is $M_{21}=2m_\uparrow+m_\downarrow$ and the atom-pair reduced mass $m_{21}^{-1}=(m_\uparrow+m_\downarrow)^{-1}+m_\uparrow^{-1}$.

Note that the interacting part of the virial coefficient in the spin- and mass-balanced case is given by $\Delta b_3 = \frac{1}{2}(B_{21}+B_{12}) = B_{21}$.

D. $\mathbf{N_\uparrow = N_\downarrow = 2}$

For two $\uparrow$ and two $\downarrow$ atoms, we write down the Green's operator, similarly to the previous cases:

$\hat{G}(E) =$ (36a)

$+ \Big($ $+ \cdots +$ $[\uparrow\leftrightarrow\downarrow]\Big)$ (36b)

$+ \Big[$ $+$ (36c)

$+ \Big($ $+$ $[\uparrow\leftrightarrow\downarrow]\Big)$ (36d)

$+$ $+ \ldots \Big]$. (36e)

Here, Eq. (36a) depicts the free part and the two-body contributions; Eq. (36b) the three-body contributions; and Eqs. (36c-36e) the four-body contributions. In (36b), the infinite diagrammatic series can be replaced by the three-body propagator, t_3, and thus can be calculated in full. On the other hand, we only write down explicitly the diagrams containing exactly three T_2's in Eq. (36c) and four T_2's in Eqs. (36d-36e). The terms with five or more T_2's are omitted here and in the following. While not completely general, this may be shown to correspond to a perturbative approach (the Born approximation) in certain limits, as discussed in Sec. II, and explicitly shown in IV.

To obtain the virial coefficient, one follows the framework outlined in previous sections. All relevant diagrams can be obtained by keeping only the connected diagrams resulting from the trace of the Green's operator under the exchange operator. We note however that the third term in Eq. (36a) contains identical two-atom sub-clusters and thus a factor of 1/2! is required to avoid over counting.

E. $\mathbf{N_\uparrow = 3}$; $\mathbf{N_\downarrow = 1}$

Here we consider the other possible interacting four-body cluster – three $\uparrow$ and one $\downarrow$ atoms (there is, of course, an equivalent diagram with three $\downarrow$ and one $\uparrow$ atoms). As before, we write down the Green's operator of this few-body system

$\hat{G}(E) =$ $+$ $+ \Big[$ $+$ $+ \ldots \Big]$ (37a)

$+ \Big[$ $+$ $+ \ldots \Big]$. (37b)

In Eq. (37a), the first term denotes the free propagator; the second the two-body contribution; and the terms in the bracket the three-body contributions which can be calculated exactly by means of the STM integral equation. The four-body contribution is written down in Eq. (37b) where the diagrams containing more than four T_2's are omitted. Again we note that this can be shown to correspond to a perturbative approach in certain limits.

All relevant diagrams can be obtained by applying the exchange operator to the diagrams above and taking the trace. We note that the two-body diagram [the second term in Eq. (37a)] contains two identical single-particle propagators and thus a factor of 1/2! must be introduced.

IV. VIRIAL COEFFICIENTS OF THE RESONANT FERMI GAS

After the quite general discussion of the virial expansion above, we now confine ourselves to the specific case of a spin- and mass-balanced Fermi gas in three dimensions, described by the Hamiltonian (1) [59]. We present the second, third, and fourth virial coefficients for the resonant Fermi gas, calculated using the technique described in the preceding section. Our calculation of the fourth virial coefficient is perturbative for a narrow resonance where $T \gg 1/mR^{*2}$, and approximate in the broad resonance case. All other results are numerically exact.

A. Second virial coefficient

In the spin- and mass-balanced gas, the second virial coefficient takes the value $-2^{-5/2}$ in the absence of interactions — see Eq. (23). The part of the second virial coefficient arising from interactions can be obtained by inserting the two-body T matrix (2) in the expression for the second virial coefficient, Eq. (31). This yields

$$\Delta b_2 = \sqrt{2}\oint_E' \frac{mR^* + \frac{m}{2\sqrt{-mE}}}{a^{-1}-\sqrt{-mE}+mR^*E}. \quad (38)$$

As depicted in Fig. 2, Δb_2 increases monotonically from the Fermi regime, through unitarity, to the Bose regime.

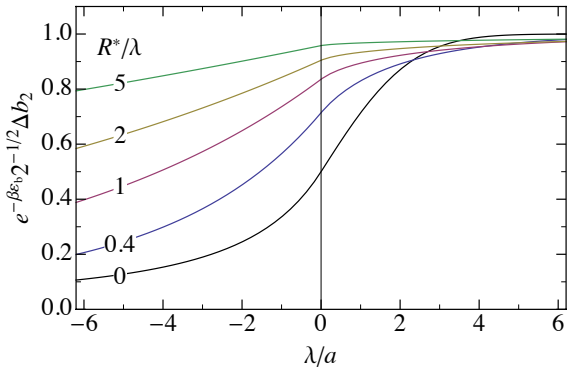

FIG. 2: The interaction part of the second virial coefficient as a function of interaction strength for several values of R^*/λ. As $\lambda/a \to \infty$ the virial coefficient approaches $\sqrt{2}e^{\beta\varepsilon_b}$ and we normalize by this factor (taking $\varepsilon_b = 0$ for $a \leq 0$).

Consider first the limits $|a| \ll \lambda$ where the temperature is much smaller than the energy scale of few-body physics. Owing to the Boltzmann factor $\exp[-\beta E]$, the leading contribution of the contour integral over E then comes from an interval of length $\sim T$ starting at the leftmost point of the non-analytic structure of the T matrix. Using this to evaluate the virial coefficient in the Fermi limit $\lambda/a \ll -1$, the asymptotic form is $\Delta b_2 = -a/\lambda + 3\pi R^* a^2/\lambda^3$ for $|a| \ll R^* \lesssim \lambda$. On the other hand, in the Bose limit $\lambda/a \gg 1$, we have $\Delta b_2 = \sqrt{2}e^{\beta\varepsilon_b} - a/\lambda$ for $R^* \lesssim \lambda$. Here, the leading term may be understood as arising from the first term of the virial expansion of a non-interacting Bose gas. Indeed, we identify the contribution to the grand potential (17) from the two interacting fermions with that of a single boson

$$-\frac{1}{\beta}\frac{2V}{\lambda^3}\Delta b_2 z^2 = -\frac{1}{\beta}\frac{V}{\lambda_{\rm Bose}^3} b_1^{\rm Bose} z_{\rm Bose}. \tag{39}$$

The factor two on the left hand side is due to the two fermionic species. Using the first virial coefficient of the ideal Bose gas, $b_1^{\rm Bose} = 1$, as well as the relation between the bosonic and fermionic chemical potentials $\mu_{\rm Bose} = 2\mu + \varepsilon_b$, the fugacity $z_{\rm Bose} = e^{\beta\mu_{\rm Bose}}$, and the thermal wavelength $\lambda_{\rm Bose} = \lambda/\sqrt{2}$, we arrive at the asymptotic form of Δb_2. We emphasize that this form of the virial coefficient implies that the system is a non-interacting Bose gas of dimers.

We next consider the evolution of Δb_2 at unitarity, as a function of R^*/λ. For broad resonances (where R^* may be taken to vanish), or for temperatures $T \ll T_{R^*} \equiv 1/mR^{*2}$, the virial coefficient takes the well-known value $1/\sqrt{2}$. On the other hand, for temperatures $T \gg T_{R^*}$ the virial coefficient is approximately $\Delta b_2 \approx \sqrt{2} - \frac{\lambda}{\pi R^*}$. This increase of the virial coefficient from $1/\sqrt{2}$ to $\sqrt{2}$ as temperature increases above the scale set by T_{R^*} has been taken to imply that the two-particle system becomes more strongly interacting [30, 37]. We, however, argue the opposite, namely that the system approaches a non-interacting limit. To understand this, it is convenient to introduce the pair propagator

$$D(E) \equiv T_2(E)/g^2 = \frac{1}{E + \frac{mg^2}{4\pi}\left(-\sqrt{-mE} + a^{-1}\right)}. \tag{40}$$

At unitarity, this has the limiting behavior

$$D(E) \sim \begin{cases} R^* E^{-1/2} & \text{if} \quad E \sim T \ll T_{R^*} \\ E^{-1} & \text{if} \quad E \sim T \gg T_{R^*} \end{cases}$$

That is, the pair propagator evolves from a resonance in the low-temperature limit into a free propagator of a zero-energy state as temperature increases beyond the energy scale set by the effective range. Thus, the two fermions simply populate this (non-interacting) pair state which, as discussed in the above paragraph, has virial coefficient $\sqrt{2}$. Indeed, the above discussion carries over to the Fermi regime where, as long as $|a| \gg R^*$, the virial coefficient becomes that of the non-interacting pair, approaching $\sqrt{2}$ as seen in Fig. 2.

B. Third virial coefficient

In the absence of interactions, the third virial coefficient in the spin- and mass-balanced gas takes the value $3^{-5/2}$; see Eq. (23). We now proceed to calculate the effect of interactions, which is encapsulated in $\Delta b_3 = B_{21}$, with B_{21} defined in Eq. (35). The calculation now requires one to solve the three-body problem in full, which has been the subject of several works in the literature. Here we mainly follow Refs. [38, 39], but see also Ref. [40] for a related framework for the calculation of the third virial coefficient. For completeness, we include a discussion of the three-body problem in Appendix A.

Consider the crossover from the Fermi to the Bose regimes, as depicted in Fig. 3. In the broad resonance case shown in Fig. 3(a), our results completely match those of Refs. [22, 23] in the whole range of interactions, and Refs. [24, 25] at unitarity. The results do not match those of Ref. [41], in which the three-body problem was confined to the s-wave channel. We first discuss the asymptotic limits in which the few-body energy scale set by the two-body scattering length is much greater than temperature, focusing on the broad resonance case for simplicity. Then, we have the scaling of the three contributions of Eq. (35) to the interaction part of the virial coefficient:

$$\frac{\lambda^3}{V}\oint_E' \; \sim \begin{cases} (\frac{a}{\lambda})e^{\beta\varepsilon_b} & \text{Bose} \\ (\frac{a}{\lambda})^2 & \text{Fermi} \end{cases} \tag{41a}$$

$$\frac{\lambda^3}{V}\oint_E' \; \sim \begin{cases} (\frac{a}{\lambda})^3 e^{\beta\varepsilon_b} & \text{Bose} \\ \frac{a}{\lambda} & \text{Fermi} \end{cases} \tag{41b}$$

$$\frac{\lambda^3}{V}\oint_E' \; \sim \begin{cases} (\frac{a}{\lambda})^3 e^{\beta\varepsilon_b} & \text{Bose} \\ (\frac{a}{\lambda})^2 & \text{Fermi} \end{cases} \tag{41c}$$

where the explicit expressions for the diagrams is clear from Eq. (35). In the Fermi limit, the scaling follows

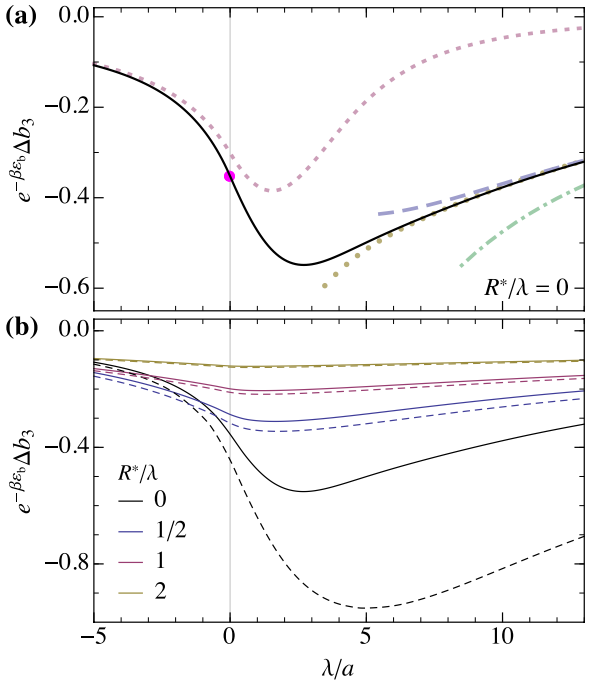

FIG. 3: The interaction part of the third virial coefficient as a function of interaction parameter. In the Bose regime the virial coefficient is proportional to $e^{\beta\varepsilon_b}$ — see Eq. (42) — and we normalize by this factor (taking $\varepsilon_b = 0$ for $a \leq 0$). (a) In the broad resonance limit, $R^*/\lambda = 0$, we compare Δb_3 (solid) with the two-body contribution which dominates in the Fermi regime (short dashed), and the results of the Beth-Uhlenbeck formula (42) including s-wave only (dot-dashed), s- and p-wave (long dashed), and up to d-wave (dotted). The circle at $\lambda/a = 0$ depicts the experimentally determined virial coefficient from Refs. [26, 27]. (b) The effect of a finite range parameter on Δb_3 (solid), and the approximation given by including only the diagrams of Eqs. (43a-c) (dashed).

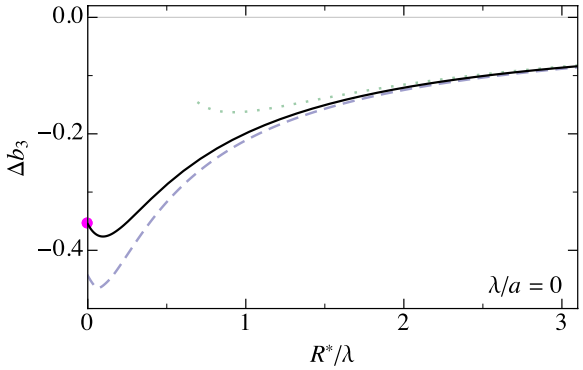

FIG. 4: The interaction part of the third virial coefficient (solid line) at unitarity as a function of R^*/λ. The dashed line depicts the result of considering only the diagrams of Eqs. (43a-c), corresponding to replacing the full three-body T matrix by its Born approximation. The dotted curve is the narrow resonance asymptote — see Eq. (44).

from all momenta and energies being set by λ. Therefore, $T_2 \sim a/m$ and $t_3 \sim m\lambda^2$. On the other hand, in the Bose limit, the Boltzmann factor in the two-body T matrix forces the energy $E = -\varepsilon_b + E_{col}$ to be within a collision energy $E_{col} \sim 1/m\lambda^2$ of the binding energy. Thus $T_2(-\varepsilon_b + E_{col}) \approx \frac{8\pi}{m^2 a}\frac{1}{E_{col}} \sim \lambda^2/ma$ and $t_3 \sim ma^2$. In Eq. (41c), due to the exchange process, two momenta are integrated over, and only one of these is suppressed by the Boltzmann factor; consequently, in this diagram the momenta count as $1/\lambda$ and $1/a$, respectively.

As may be anticipated, the two-body contribution, Eq. (41b), is the dominant contribution in the weakly interacting Fermi regime. On the other hand, in the Bose limit, Eq. (41a) is the leading contribution. This has a very natural interpretation: Due to the lack of exchange of the external legs, this diagram corresponds to atom-dimer scattering, and thus to an effective two-body process. Then we may recast the virial coefficient in Beth-Uhlenbeck form, similarly to the two-body problem in Eq. (31). The result is

$$\Delta b_3 \overset{\lambda \gg a}{\approx} 3^{\frac{3}{2}} e^{\beta\varepsilon_b} \sum_\ell \xi_\ell \int_0^\infty \frac{dk}{\pi} e^{-\beta\frac{3k^2}{4m}} \delta'_{ad,\ell}(k), \qquad (42)$$

where $\delta_{ad,\ell}$ is the atom-dimer phase shift in the ℓ'th partial wave. For details on the derivation of Eq. (42), see Appendix B. If the temperature is negligible compared with the binding energy, only the low-energy behavior of the scattering phase shifts matter, i.e., the atom-dimer scattering length $a_{ad} = -\lim_{k\to 0} k^{-1} \tan\delta_{ad,\ell}(k) = 1.18a$ [36]. For decreasing λ/a we need to take the derivative of the phase shifts obtained in Refs. [39, 42]. The result is shown in Fig. 3(a) and yields a good approximation to the virial coefficient for $\lambda/a \gtrsim 5$.

Next we investigate the behavior of the virial coefficient for a finite range parameter — see Fig. 3(b). First of all, we see that increasing R^*/λ tends to suppress the virial coefficient for fixed λ/a. Secondly, we see that a perturbative approach works very well already at $R^*/\lambda = 1$. The particular approach we use is to take the first Born approximation of the three-body T matrix, i.e., keeping only the first term in Eq. (34). That is, the three diagrams contributing to Δb_3 take the form:

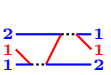

$$= -\sum_{\mathbf{p}} \frac{T_2^2(E-\frac{3p^2}{4m})\frac{dT_2^{-1}(E-\frac{3p^2}{4m})}{dE}}{E-\frac{3p^2}{m}}, \qquad (43a)$$

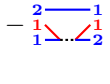

$$= -\sum_{\mathbf{p}} \frac{T_2(E-\frac{3p^2}{4m})}{\left(E-\frac{3p^2}{m}\right)^2}, \qquad (43b)$$

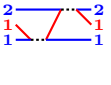

$$= \sum_{\mathbf{p},\mathbf{p}'} \frac{T_2(E-\frac{3p^2}{4m})T_2(E-\frac{3p'^2}{4m})}{(E-\epsilon_{\mathbf{p}}-\epsilon_{\mathbf{p}'}-\epsilon_{\mathbf{p}+\mathbf{p}'})^3}. \qquad (43c)$$

The idea is that keeping the exact pole structure of the two-body T matrix may help control the approximation

in the regime where $R^* \sim \lambda$. The close agreement between the exact calculation and our approximation observed in Fig. 3(b) appears to validate our approach. The main difference between the perturbative approach and the exact takes place for a broad resonance in the Bose regime: The source of the discrepancy is that for a broad resonance the Born approximation of atom-dimer scattering predicts $a_{\rm ad} = 8a/3$, while the exact calculation gives $a_{\rm ad} = 1.18a$ [36], and thus the atom-dimer interaction is overestimated in the Born approximation. We further illustrate the comparison between the exact, approximate (in the above sense), and truly perturbative (expanding $T_2(E)$ in powers of $1/R^*$) approaches in Fig. 4. It is seen that our approximation provides a very good agreement with the exact virial coefficient, even as R^*/λ approaches zero. We find the exact value at $R^* = 0$ to be $\Delta b_3 \simeq -0.3551$, in agreement with Refs. [22, 23, 25].

Finally, we note that Δb_3 at unitarity is non-monotonic as a function of R^*/λ, a feature which is present in both the exact and approximate results — see Fig. 4. This reflects how at small R^*/λ a new interaction channel becomes available, increasing the magnitude of the virial coefficient, whereas at large R^*/λ the interactions are suppressed. In the limit $R^*/\lambda \gg 1$ we evaluate the asymptotic form of the virial coefficient:

$$\Delta b_3 \overset{\lambda \ll R^*}{\approx} -\frac{2\sqrt{2}}{3\pi}\frac{\lambda}{R^*} + \frac{4(5\sqrt{3}\pi - 18)}{27\pi^2}\left(\frac{\lambda}{R^*}\right)^2 . \quad (44)$$

In Fig. 4 we see that this asymptotic expression works very well for $R^*/\lambda \gtrsim 2$.

C. Fourth virial coefficient

In the absence of interactions, the fourth virial coefficient takes the value: $b_4^{\rm free} = -4^{-5/2}$. In order to obtain the contribution to the virial coefficient arising from interactions, one may in principle extend the above diagrammatic analysis; however the task of solving the four-body problem exactly is numerically taxing. Instead, we take a pragmatic approach and consider the Born approximation of the four-body problem, summing all diagrams containing at most four two-body propagators. This includes the first Born approximation of the dimer-dimer scattering T matrix. The relevant diagrams are shown in subsections III D and III E. This is the same approximation which was shown above to work very well for Δb_3 once $R^*/\lambda \geq 1$; at unitarity, it even gave a reasonable result once $R^* \to 0$. The two- and three-body contributions to Δb_4 are computed exactly.

Figure 5(a) depicts the virial coefficient within our approximation for a broad resonance with $R^*/\lambda = 0$. We see that in the weakly interacting Fermi limit of $\lambda/a \ll -1$, the two-body contribution dominates. On the other hand, in the Bose limit where $\lambda/a \gg 1$, the four fermions may be approximated by two deeply bound dimers. The virial coefficient is then a sum of a contribution arising from the second-order term of a non-interacting Bose gas, and one from the dimer-dimer interaction. Employing for the former the same arguments which related the second virial coefficient of the Fermi gas with the first of a non-interacting Bose gas, see Eq. (39), and for the latter the same arguments which lead to the Beth-Uhlenbeck expression for the third virial coefficient in the Bose regime, Eq. (42), we find

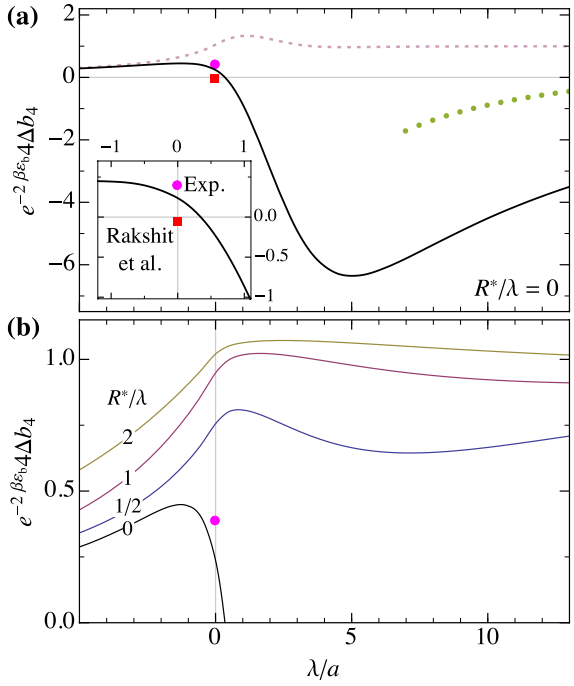

FIG. 5: The interaction part of the fourth virial coefficient as a function of the interaction parameter λ/a. In the Bose regime, $\Delta b_4 \to e^{2\beta\varepsilon_b}/4$ and we normalize by this factor, taking $\varepsilon_b = 0$ for $a \leq 0$. (a) For a broad resonance with $R^*/\lambda = 0$ we display our approximate value of Δb_4 (solid), along with the dominant two-body contribution in the Fermi regime (short dashed), and the dominant contribution in the Bose limit, Eq. (45), taking $a_{\rm dd} \approx 0.6a$ (dotted). The circle represents the experimental measurement [26, 27] and the square the calculation of Ref. [25]. (b) Taking the effective range into account, we display the virial coefficient for $R^*/\lambda = 0$, 1/2, 1, 2 (bottom to top).

$$\Delta b_4 \overset{\lambda \gg a}{\approx} e^{2\beta\varepsilon_b}\left[\frac{1}{4} + 8\sum_\ell \xi_\ell \int_0^\infty \frac{dk}{\pi} e^{-\beta\frac{k^2}{2m}}\delta'_{{\rm dd},\ell}(k)\right]$$
$$\approx e^{2\beta\varepsilon_b}\left(\frac{1}{4} - 8\frac{a_{\rm dd}}{\lambda}\right), \quad (45)$$

where we approximate $-k^{-1}\tan\delta_{{\rm dd},0}(k) \approx a_{\rm dd}$ and ignore all phase shifts other than s-wave. The correct dimer-dimer scattering length is $a_{\rm dd} = 0.6a$, as derived in Ref. [33]; for a diagrammatic derivation closer to the present formulation, see Refs. [43, 44]. We see that the asymptote (45) gives a much smaller dimer-dimer interaction shift of the virial coefficient compared to our approximate result. This is because our approach contains

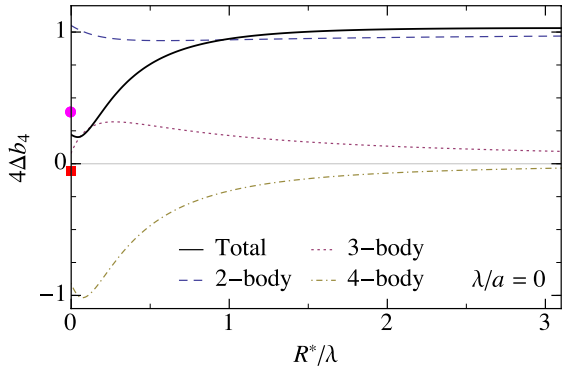

FIG. 6: The interaction part of the fourth virial coefficient at unitarity ($1/a = 0$) as a function of the effective range R^*/λ. The four-body contribution to the virial coefficient is approximated as explained in the text.

only the leading diagram of the Born approximation of dimer-dimer scattering, which overestimates the dimer-dimer repulsion and yields $a_{\rm dd} = 2a$. Nevertheless, we expect our result to recover the qualitative behavior of Δb_4 across the crossover. In particular, we see that the coefficient is positive in the Fermi regime and changes sign close to unitarity mainly due to the dimer-dimer repulsion at large positive λ/a. Finally, it changes sign again and becomes positive — using $a_{\rm dd} = 0.6a$ in Eq. (45) we estimate this to occur for $\lambda/a \approx 19$.

Increasing the range parameter for fixed scattering length suppresses the dimer-dimer interaction — see Ref. [39]. Consequently, as shown in Fig. 5(b), already at $R^*/\lambda = 1/2$ we do not expect that the virial coefficient changes sign in the crossover. As in the three-body case, we expect the virial coefficient calculated within our approximation to work well once $R^*/\lambda \geq 1$.

Consider finally the unitary Fermi gas, where we find $\Delta b_4 \approx 0.06$ for a broad resonance — see Fig. 6. This is in contrast to the previous theoretical work of Ref. [25], where Δb_4 was found to be negative [60]. We note however that our Δb_4 is still smaller than the experimental value $\Delta b_4^{\rm exp.} \approx 0.096$ [26, 27], most likely due to the overestimation of the dimer-dimer repulsion within our approximation. Our results also illustrate the difficulty in determining the fourth virial coefficient, as the coefficient is expected to show a strong non-monotonic behavior in the vicinity of the resonance. For large R^*/λ we see that the two-body contribution to the virial coefficient dominates and $\Delta b_4 \to 1/4$. This is again an illustration of how the system evolves towards a non-interacting Bose gas in this limit. The first correction to this result arises from both two- and the three-body contributions, and we find the limiting behavior

$$\Delta b_4 \overset{\lambda \ll R^*}{\approx} \frac{1}{4} + \frac{9-4\sqrt{3}}{12\pi}\frac{\lambda}{R^*}, \tag{46}$$

for a narrow resonance at unitarity.

D. Higher virial coefficients in the Fermi and Bose regimes

It is clear from the preceding discussion that the interaction part of the virial coefficient in the weakly interacting Fermi regime is dominated by the two-body contribution, i.e., for $\lambda/a \ll -1$ we have $\Delta b_N \approx \Delta b_N^{\text{2-body}}$. For reference, we give this here up to arbitrary order

$$\Delta b_N^{\text{2-body}} = \frac{(-1)^N}{N^{5/2}} \oint_E{}' \frac{\frac{m}{\pi} T_2(E)}{\sqrt{-mE}} \sum_{j=0}^{N-2} (N-j-1) \times \left[e^{\zeta_N}(1+2\zeta_N)\left(1+\text{Erf}\left[-\sqrt{\zeta_N}\right]\right) - \frac{2\sqrt{\zeta_N}}{\sqrt{\pi}} \right], \tag{47}$$

where $\zeta_N = -\beta E[N-2-\frac{1}{N}(N-2j-2)^2]/2$.

In the opposite limit where $\lambda/a \gg 1$, the virial coefficients Δb_N are related to those of a non-interacting Bose gas. Specifically, as $\lambda/a \to \infty$ the virial coefficients approach

$$e^{-\frac{N}{2}\beta\varepsilon_{\rm b}} \Delta b_N \to \sqrt{2} \begin{cases} b_{N/2}^{\rm Bose} = (N/2)^{-5/2} & N \text{ even} \\ 0 & N \text{ odd} \end{cases}. \tag{48}$$

This result holds even at unitarity when $R^*/\lambda \gg 1$. For even N, this formula follows from comparing the contributions to the grand potential from N interacting fermions with that of $N/2$ non-interacting bosons, as in the case of the second virial coefficient — see Eq. (39).

The asymptotic form of the virial coefficients in the Bose limit where the virial coefficients grow exponentially, Eq. (48), prompts us to define the effective fugacity

$$z^* = \begin{cases} z & \text{if} \quad a \leq 0 \\ e^{\beta\varepsilon_{\rm b}/2} z & \text{if} \quad a > 0 \end{cases}, \tag{49}$$

such that all coefficients in the power series in z^* remain of order unity throughout the crossover.

V. THERMODYNAMICS

Having calculated the virial coefficients, we now turn to the investigation of the thermodynamics of the resonant Fermi gas. In the grand canonical ensemble, the thermodynamic variables of a homogeneous system are functions of the chemical potential, temperature, and volume. That is, the grand potential is $\Omega = \Omega(\mu, T, V)$ from which all thermodynamic variables can be obtained. The pressure is given by

$$P = -\frac{\Omega}{V} = P_0 + 2T\lambda^{-3} \sum_{N\geq 2} \Delta b_N z^N, \tag{50}$$

where the ideal Fermi gas pressure is given by $P_0 = 2T\lambda^{-3}[-\text{Li}_{5/2}(-z)]$, with Li_ν the polylogarithm. The

density reads

$$n = -\left.\frac{\partial}{\partial\mu}\frac{\Omega}{V}\right|_{T,V} = n_0 + \frac{2}{\lambda^3}\sum_{N\geq 2} N\Delta b_N z^N, \qquad (51)$$

where $n_0 = 2\lambda^{-3}[-\mathrm{Li}_{3/2}(-z)]$ is the density of an ideal Fermi gas. Finally, we write down the entropy density $s \equiv S/V$:

$$s = -\left.\frac{\partial}{\partial T}\frac{\Omega}{V}\right|_{\mu,V} = \frac{5}{2}\frac{P}{T} - \frac{\mu}{T}n + \frac{2}{\lambda^3}\sum_{N\geq 2} T\frac{\partial\Delta b_N}{\partial T} z^N. \qquad (52)$$

Note that we only have $\partial\Delta b_N/\partial T$ appearing in s since the ideal Fermi gas virial coefficients do not depend on temperature.

In Fig. 7 we display the pressure, density, and entropy for a broad resonance in the Fermi regime, at unitarity, and in the Bose regime. We see from the comparison between the second and fourth-order results that the virial expansion breaks down as z^* approaches 1, as expected. In the Fermi regime where $\lambda/a \ll -1$, the virial coefficients are dominated by those of the ideal Fermi gas, the leading correction due to interactions arising from the two-body contributions (47). In the figure, this approximation is seen to give a clear improvement compared with the second-order virial expansion. On the other hand, in the Bose regime where $\lambda/a \gg 1$, the virial coefficients are dominated by those arising from the non-interacting gas of dimers, Eq. (48), and we have

$$P \approx 2\sqrt{2}T\lambda^{-3}\mathrm{Li}_{5/2}(z^{*2}), \qquad (53a)$$

$$n \approx 4\sqrt{2}\lambda^{-3}\mathrm{Li}_{3/2}(z^{*2}), \qquad (53b)$$

$$s \approx \sqrt{2}\lambda^{-3}\left[5\mathrm{Li}_{5/2}(z^{*2}) - 2\beta(2\mu+\varepsilon_\mathrm{b})\mathrm{Li}_{3/2}(z^{*2})\right]. \qquad (53c)$$

The leading correction arises from the dimer-dimer scattering length contribution to Δb_4 — see Eq. (45). We do not display the Bose limit expressions in the figure, as we see from Fig. 5(a) that these are not expected to be accurate for the broad resonance until larger λ/a.

We see in Fig. 7(a) that, contrary to what one might naively expect, the pressure appears to increase as we go from the Fermi to the Bose regime. The point is that this happens at a fixed expansion parameter, causing the density to increase simultaneously, as seen in Fig. 7(b). This effect may also be understood as arising from the fact that the grand potential Ω decreases from the Fermi to the Bose regime, due to the formation of pairs.

In Fig. 8, we consider the behavior of the thermodynamic variables at unitarity as a function of the range parameter, R^*/λ. As discussed in Sec. IV, in the narrow resonance limit we may relate the virial coefficients of the two-component Fermi gas with those of a non-interacting Bose gas of pairs at zero energy. Thus the thermodynamic variables at unitarity become those of Eqs. (53a-c), where in this case $z^* = z$. We see that,

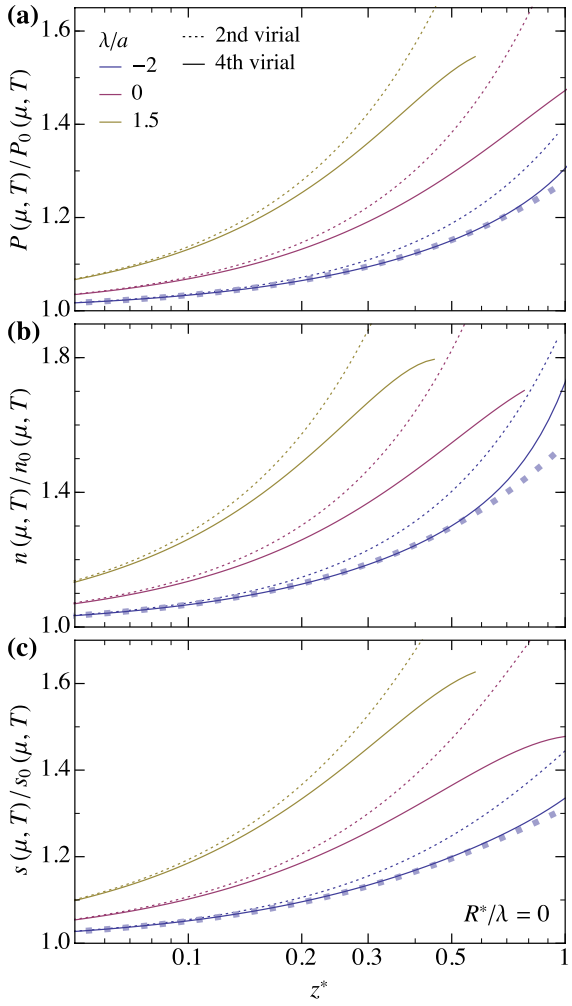

FIG. 7: The pressure P, density n, and entropy density s in the grand canonical ensemble as a function of expansion parameter z^* for a broad resonance $R^* = 0$. We compare the results from the virial expansion at second and fourth order in the fugacity, for three different values of the interaction parameter λ/a: From top to bottom we consider the Bose regime with $\lambda/a = 1.5$, unitarity, and the Fermi regime with $\lambda/a = -2$. For the latter, the virial coefficients are dominated by the two-body contribution (47), the result of which is shown as a thick dashed line.

as R^*/λ increases, the thermodynamic variables quickly approach those of the non-interacting Bose gas. This further underlines how the narrow resonance limit is not strongly interacting. We also see that the virial expansion appears to work better in the narrow resonance limit, i.e., the second-order result becomes closer to the fourth-order result. This is mainly because the odd orders of the expansion (e.g., third order) are suppressed as the system evolves into a non-interacting gas of dimers.

In Fig. 9, we compare the virial expansion of the pressure and density to the experimental data from the MIT experiment [27], which was conducted for a broad resonance in the unitary limit, $1/a = 0$. Although our ap-

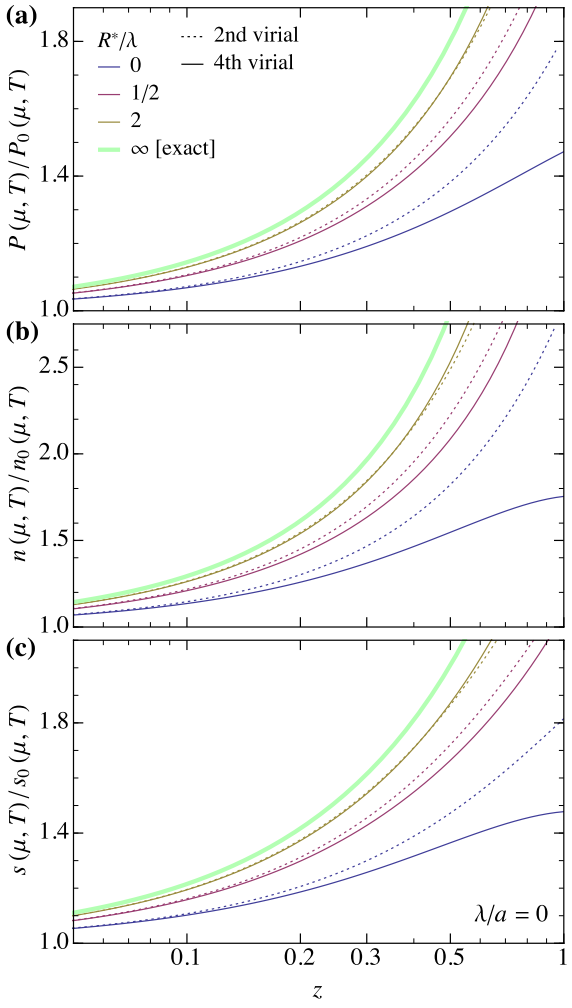

FIG. 8: The pressure, density, and entropy at resonance. We compare the second and fourth orders of the virial expansion for various resonance widths. In the narrow resonance limit, the limiting behavior of the thermodynamic variables is given in Eqs. (53a-c).

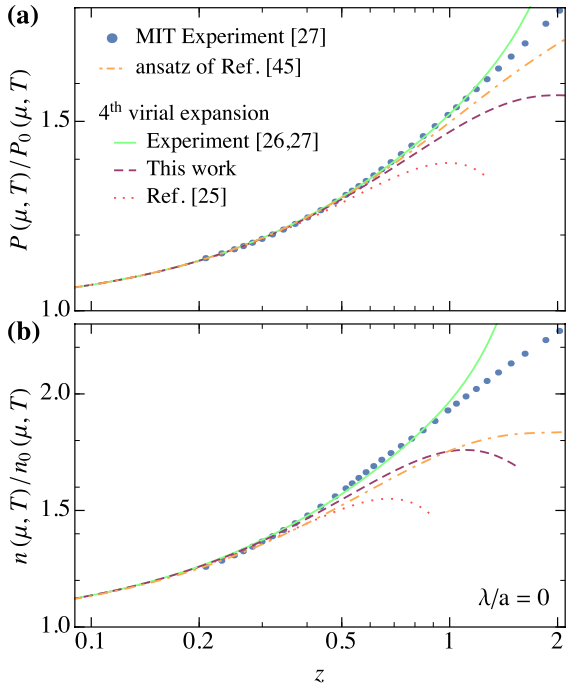

FIG. 9: Comparison between experiment [27] and various theories for the pressure and density at unitarity for a broad resonance.

proximation for the interaction part of the fourth virial coefficient, $\Delta b_4^{\rm Born} \approx 0.06$, is smaller than the best fit to the experimental data, $\Delta b_4^{\rm exp.} \approx 0.096$ [26, 27], we observe a clear improvement when comparing to the result of the previous theoretical estimate which had a negative sign [25]. We also apply the results of the virial expansion ansatz developed in Ref. [45] up to 20th order in the fugacity, and this approach is seen to work quite well for the pressure and somewhat worse for the density. Finally, we would like to point out that the fourth virial coefficient may even be slightly larger than the reported value of 0.096, as this would provide a better fit to the experimental data in the region around $z \sim 0.5$, particularly in the case of the density. The fit as one approaches $z = 1$ is less important since any deviation of the fourth-order virial expansion can be easily compensated by the inclusion of higher orders of the virial expansion.

Thus far, we have worked in the grand canonical ensemble. This is quite natural in ultracold atomic gases, where the chemical potential across the external trap can typically be treated in the local density approximation, $\mu(r) = \mu - V_{\rm ext}(r)$. However, in a uniform system it is often advantageous to consider the density instead of the chemical potential. It is then convenient to work in the canonical ensemble, where the relevant thermodynamic potential is the Helmholtz free energy $F = F(n, T, V)$. In practice, one fixes the density and solves for the fugacity using Eq. (51), where the power series in fugacity is truncated at a chosen order. When determing thermodynamic quantities P, s, we only truncate the contribution arising from interactions and we treat the ideal gas contribution exactly, i.e., the quantity $\Delta\Omega \equiv \Omega - \Omega_0$ is expanded instead of the grand potential Ω. The advantage of this approach is that we recover the ideal Fermi gas to all orders in the Fermi limit. However, the different truncation schemes should not lead to significantly different results when the fugacity is small, which is a required condition for the virial expansion.

To determine the region of validity of the virial expansion in this parameter space, we calculate the fugacity as a function of temperature T/T_F and interaction strength $1/k_F a$ using the virial expansion up to third order. Here, $T_F = \varepsilon_F = \frac{k_F^2}{2m}$, with T_F and ε_F the Fermi temperature and energy, respectively. In Fig. 10, we see that the effective expansion parameter z^*, defined in Eq. (49), becomes comparable to unity for temperatures $T \sim T_F$, as expected, and thus one should apply the virial expansion at a lower temperature with some

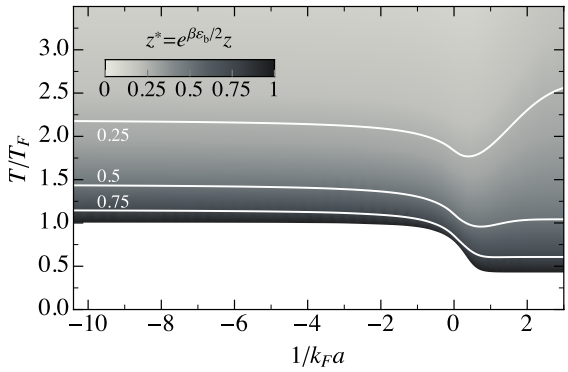

FIG. 10: Contour plot of the effective fugacity z^* in the T/T_F versus $1/k_Fa$ plane for a broad resonance with $R^* = 0$. The high-temperature expansion is considered up to the third virial coefficient, since our Born approximation for the fourth virial coefficient overestimates the effective dimer-dimer repulsion in the Bose regime. Note that we observe qualitatively similar behavior for a narrow resonance, and also if we limit ourselves to the virial expansion up to second order in the fugacity.

care. In addition, we note that at a given temperature T/T_F, z^* has a minimum on the Bose side near unitarity, corresponding to the point where the atomic and molecular states are roughly equally accessible, and the density is spread between these states. Further into the Bose (Fermi) regimes, the density of dimers (atoms) builds up and the system approaches quantum degeneracy.

Figure 11(a) depicts the crossover behaviour of the pressure and entropy density for various temperatures and range parameters. We see how in the Fermi regime $1/k_Fa \lesssim -1$, these thermodynamic quantities are close to those of the ideal Fermi gas, whereas in the opposite regime they approach those of the ideal Bose gas. Note that our results deviate from the expected value in the Bose limit because the virial expansion we use only determines the interaction part up to second order in z and therefore we only calculate the Bose gas up to first order in $z_{\rm Bose}$. The crossover to tightly bound dimers occurs when the binding energy $\varepsilon_{\rm b} \gg k_BT\log(\sqrt{2}/n\lambda^3)$, as discussed previously. Interestingly, for a given T/T_F, this crossover point can be connected with particular values of P/P_0 and s/s_0, which appear to stay roughly constant as we vary R^*.

VI. SPECTRAL FUNCTION

Finally, we consider the spectral function $A(\mathbf{k},\omega) = -2\Im G(\mathbf{k},\omega)$. This quantity is of great practical relevance, as it may be probed in cold atom experiments by the use of radio-frequency spectroscopy, allowing a direct investigation of many-body effects. For instance, Ref. [6] used this technique to observe the formation of a pairing gap both above and below the critical temperature for superfluidity. A typical experiment starts from the strongly-interacting state, and applies a radio-frequency pulse to transfer one of the $\uparrow,\downarrow$ spin states into an initially unoccupied state. In the absence of interactions between the final and initial spin states, the transfer rate is

$$I(\mathbf{k},\omega) \propto n_F(\omega)A(\mathbf{k},\omega),$$

within linear response. Here, the Fermi distribution $n_F(\omega) = (e^{\beta\omega}/z+1)^{-1}$ accounts for the probability of the initial state being occupied. As usual, the Dyson equation $G^{-1} = G_0^{-1} - \Sigma$ links the interacting with the non-interacting single-particle Green's function. The self energy can be expanded in powers of fugacity (see for instance Refs. [46, 47]), and the lowest order contribution is

$$\Sigma(\mathbf{k},\omega) = z\sum_{\mathbf{q}} e^{-\beta\epsilon_{\mathbf{q}+\mathbf{k}}} T_2\left(\omega+\mu-\epsilon_{\mathbf{k}}+\frac{\epsilon_{\mathbf{q}}}{2}\right). \quad (54)$$

The transition rate $I(\mathbf{k},\omega)$ is illustrated in Fig. 12. In the absence of interactions this would simply correspond to a narrow peak at the free dispersion, indicated by a dashed white line in the figures. However, interactions broaden the peak and profoundly modify the spectrum: For positive scattering length, we see that the spectral function develops a gap which separates the lower band associated with paired atoms from the sharper upper peak corresponding to unpaired atoms. Furthermore, the atomic peak is seen to shift upward (downward) for sufficiently large positive (negative) scattering lengths. We also consider the effect of a finite effective range. Here, we clearly see that the atomic peak becomes sharper and approaches the free dispersion, even at unitarity. This once again indicates that the system approaches a non-interacting limit for increasing k_FR^*.

VII. CONCLUSION

In this work, we have developed a diagrammatic formalism for computing the coefficients of the virial expansion, and we have used it to elucidate the high-temperature behavior of the resonant Fermi gas. We have focussed on the crossover from the regime of unpaired atoms to the regime of strongly bound pairs, and described the corresponding limiting behaviors of the virial coefficients and thermodynamics. While the unitarity point is special in the sense that it is non-perturbative in a and independent of an interaction length scale for a broad resonance, it is still possible to estimate values of the thermodynamic variables at this point since all virial coefficients are continuous functions of λ/a and R^*/λ throughout the crossover. In particular, our approximate calculation of the fourth virial coefficient for a broad resonance is likely to be qualitatively very similar to the exact result, being an interpolation between known limits. Likewise, we believe our result of $\Delta b_4 \approx 0.06$ for the fourth virial coefficient at unitarity is close to the

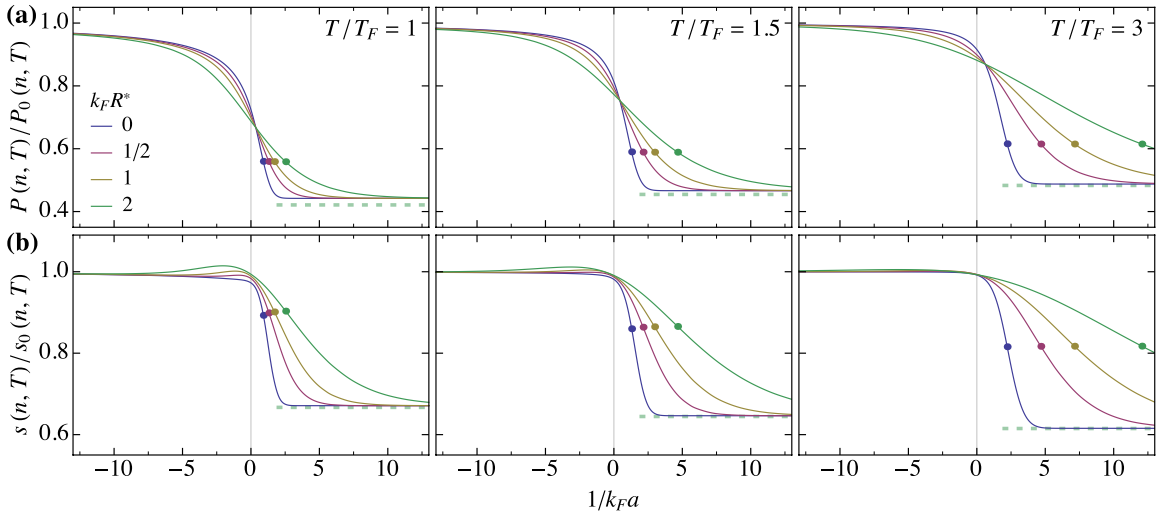

FIG. 11: The crossover behaviour of the pressure P and entropy density s for both broad and narrow resonances. The solid lines correspond to the results of the virial expansion where the non-interacting Fermi gas contribution is treated exactly while the interacting part is only calculated up to the second virial coefficient. The solid circles mark the Fermi-Bose crossover point where $n\lambda^3 \approx \sqrt{2}e^{-\beta\varepsilon_b}$. The dashed lines illustrate the thermodynamic values expected for an ideal Bose gas of dimers.

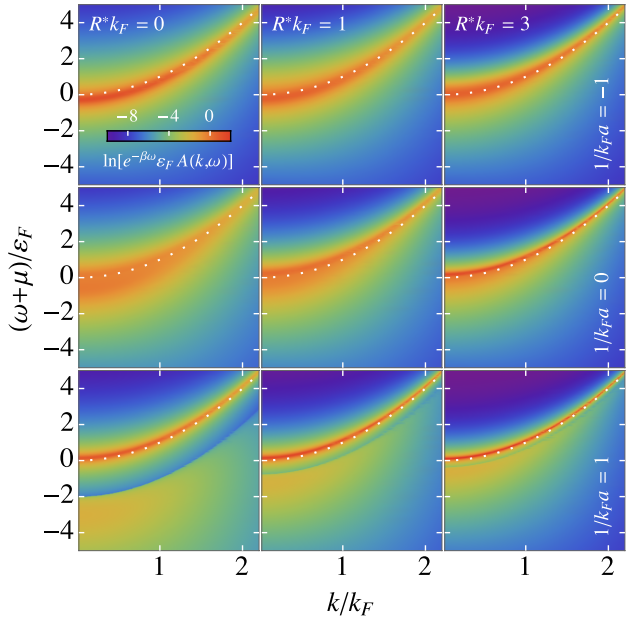

FIG. 12: The occupied part of the spectral function for various values of the interaction parameter $1/k_F a$ (top-to-bottom) and effective range $k_F R^*$ (left-to-right) near the crossover. They all correspond to the expansion parameter $ze^{\beta\varepsilon_b/2} \approx 0.2$. The short-dashed line corresponds to the free particle dispersion.

(currently unknown) exact value, and indeed it compares favorably with current experiment. However, the strong non-monotonic behavior close to the resonance also explains why it has been difficult to determine this coefficient accurately.

We have also explored the behavior of the virial coefficients once a finite effective range is introduced. Here we have shown that the coefficients can be determined perturbatively, and we have calculated the third and fourth virial coefficients for the first time. We have argued that the narrow resonance limit $R^* \gg \lambda$ corresponds to a non-interacting mixture of closed-channel molecules and atoms. We have illustrated this point by considering the behavior of the virial coefficients, thermodynamic variables, and the spectral function. This should be contrasted to the interaction energy which, for a resonant gas at zero temperature, indeed increases with increasing $k_F R^*$ [30]. However, this phenomenon is simply due to the depletion of the Fermi sea as non-interacting pairs with zero energy are formed, and we consider this to be a trivial pairing effect.

The formalism we have developed for the virial expansion is quite general and is written in Section III for a generic short-range interaction in d dimensions, for any mass ratio, and for any spin imbalance. Thus, there are a number of immediate extensions to our work on the resonant Fermi gas. For instance, one could consider the spin-imbalanced gas, where there are now two expansion parameters due to the two different chemical potentials, $\mu_\uparrow > \mu_\downarrow$. In this case, the high-temperature crossover should be considered as a crossover from a Fermi-Fermi mixture with expansion parameters $e^{\beta\mu_\uparrow}$ and $e^{\beta\mu_\downarrow}$, to a Bose-Fermi mixture described by effective expansion parameters $e^{\beta(\mu_\uparrow+\mu_\downarrow+\varepsilon_b)}$ and $e^{\beta\mu_\uparrow}$, assuming that $\mu_\uparrow - \mu_\downarrow$ is comparable to ε_b in this limit.

One can expect even richer behavior from the mass-imbalanced system due to the possibility of additional scattering resonances. We have already described how the third and the fourth virial coefficients in the Bose regime $\lambda/a \gg 1$ may be related to the derivatives of the low-energy atom-dimer and dimer-dimer scattering

phase-shifts, respectively. Whenever the few-body system is near-resonant, these derivatives will change from 0 to $\pi/2$ over a small energy range compared with the dimer binding energy, and consequently the virial coefficients can be enhanced close to the formation of few-body bound states, as discussed in Refs. [21, 48]. In particular, one expects an enhancement of the p-wave contribution to the virial coefficient B_{21} when $m_\uparrow/m_\downarrow$ approaches 8.2, the critical value for the formation of trimers in the p-wave channel when $a \gg R^*$ [49]. Even below the critical mass ratio, such as in a potassium-lithium mixture with mass ratio 40/6, the atom-dimer scattering is strongly enhanced, as discussed in Refs. [39, 42] and demonstrated in a recent experiment [50]. Likewise, tetramers are predicted to exist in the $\uparrow\uparrow\uparrow\downarrow$ problem [51, 52] leading to an enhancement of the coefficient B_{31} close to the critical mass ratio of 9.5 close to unitarity [52]. Indeed, the sign-change of the third virial coefficient at unitarity as a function of mass ratio [53] results from the resonantly enhanced p-wave channel becoming dominant. Thus, few-body effects can profoundly impact the normal state of a heteronuclear Fermi gas.

Finally, one may consider particles with other statistics. Thus far, the virial expansion of the Bose gas has only been developed up to the third virial coefficient at unitarity [54], the results showing an intriguing dependence on the three-body parameter introduced by Efimov physics [55]. It would thus be interesting to consider the behavior across resonance, as in the present work.

Acknowledgments

We would like to thank Xavier Leyronas for discussions, and Martin Zwierlein for the data of Ref. [27]. V.N. wishes to thank Aarhus Institute of Advanced Studies for hospitality during part of this work. M.M.P. acknowledges support from the EPSRC under Grant No. EP/H00369X/2.

Appendix A: Three-body problem

The three-body problem with short-range interactions is described completely by the Skorniakov–Ter-Martirosian (STM) integral equation. Originally introduced to calculate neutron-deuteron scattering length [36], the diagrammatic representation of the STM equation reads (see also Ref. [38, 39])

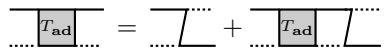

(A1)

Here $T_{\rm ad}$ is the atom-dimer scattering T matrix; the solid lines denote free atom propagators and the dotted lines the two-body T matrix. We then write Eq. (A1) for an $\uparrow\uparrow\downarrow$ system as an integral equation

$$T_{\rm ad}(\mathbf{k},k_0;\mathbf{p},p_0;E) = \zeta\Bigg[g^2 Z G_\downarrow(-\mathbf{k}-\mathbf{p},E-k_0-p_0) - \int\frac{d^3\mathbf{q}}{(2\pi)^3}\int\frac{dq_0}{2\pi i}G_\uparrow(\mathbf{q},q_0)G_\downarrow(-\mathbf{p}-\mathbf{q},E-p_0-q_0)T_2(-\mathbf{q},E-q_0)T_{\rm ad}(\mathbf{k},k_0;\mathbf{q},q_0;E)\Bigg]. \tag{A2}$$

We let the incoming [outgoing] atom and dimer have four-momenta $(\mathbf{k},\epsilon_\mathbf{k})$ and $(-\mathbf{k},E-\epsilon_\mathbf{k})$ [$(\mathbf{p},\epsilon_\mathbf{p})$ and $(-\mathbf{p},E-\epsilon_\mathbf{p})$], respectively. The free atom propagators is given by $G_{\uparrow,\downarrow}(\mathbf{k},k_0) = (k_0 - k^2/2m_{\uparrow,\downarrow} + i0)^{-1}$ and $T_2(\mathbf{q},q_0) \equiv T_2(q_0 + q^2/2(m_\uparrow+m_\downarrow)+i0)$ is the two-body T matrix. The residue at the pole of the two-body T matrix — $g^2 Z \equiv \lim_{s\to 0} s \times T_2(-\varepsilon_{\rm b}+s)$ — is included for correct normalization of the external dimer propagators. The factor ζ in Eq. (A2) describes the quantum statistics and is equal to -1 for the fermionic case, $+1$ for heteronuclear bosons, and $+2$ for identical bosons.

The integration over q_0 can be done by closing the contour in the lower half plane. This encloses one pole coming from $G_\uparrow(\mathbf{q},q_0)$ at $q_0 = \epsilon_\mathbf{q}$. Next, we take the partial wave projection and use the on-shell conditions: $k_0 = \epsilon_\mathbf{k}$ and $p_0 = \epsilon_\mathbf{p}$. The equation (A2) becomes

$$T_{{\rm ad},\ell}(k,p;E) = \zeta\Bigg[g^2 Z g_\ell(k,p;E) + \sum_q g_\ell(p,q;E)T_2(E-q^2/2m_{21})T_{{\rm ad},\ell}(k,q;E)\Bigg]. \tag{A3}$$

where $m_{21}^{-1} = m_\uparrow^{-1} + (m_\uparrow+m_\downarrow)^{-1}$.

The partial wave projection is defined as follows (energy omitted)

$$T_{\mathrm{ad},\ell}(p,q) = \int_{-1}^{1} \frac{dx}{2} P_\ell(x) T_{\mathrm{ad}}(\mathbf{p},\mathbf{q}),$$
$$T_{\mathrm{ad}}(\mathbf{p},\mathbf{q}) = \sum_{\ell\geq 0} (2\ell+1) P_\ell(x) T_{\mathrm{ad},\ell}(p,q), \tag{A4}$$

where $x = \cos(\hat{\mathbf{p}}\cdot\hat{\mathbf{q}})$ and $P_\ell(x)$ denote the Legendre polynomials. Similarly, one may write down the partial-wave projected $\downarrow$ propagator,

$$g_\ell(p,q) = \int_{-1}^{1} \frac{dx}{2} P_\ell(x) G_\downarrow(\mathbf{p}+\mathbf{q}, E-\epsilon_{\mathbf{p}}-\epsilon_{\mathbf{q}})$$
$$= \frac{m_\downarrow}{pq} Q_\ell\left[\frac{m_\downarrow}{pq}\left(E-\frac{p^2+q^2}{2m_r}\right)\right], \tag{A5}$$

where $Q_\ell(z) = \int_{-1}^{1}(z-x)^{-1}P_\ell(x)\,dx/2$ is the Legendre function of the second kind.

In general, there might not exist a two-body bound state, e.g., when $a<0$ in 3D. It is thus useful to define the three-body T matrix $t_3 \equiv T_{\mathrm{ad}}/g^2Z$ such that the external dimer propagators are removed from Eq. (A1). Therefore, we have

$$t_{3,\ell}(k,p;E) = \zeta\Bigg[g_\ell(k,p;E)$$
$$+\sum_q g_\ell(p,q;E) T_2(E-q^2/2m_{21}) t_{3,\ell}(k,q;E)\Bigg]. \tag{A6}$$

Appendix B: Beth-Uhlenbeck expression for Δb_3 in the Bose regime

In the Bose limit, the three-body problem reduces to the much simpler atom-dimer scattering problem. This is effectively a two-body problem and thus one may readily modify the Beth-Uhlenbeck formula, see Eq. (32), to obtain the third virial coefficient. Indeed, we have shown that the dominant diagram in this limit is the one describing atom-dimer scattering – see, Eq. (41a). That is, we have

$B_{21} \overset{\lambda\gg a}{\approx} \frac{\lambda^3}{V}\oint_E{}' $ 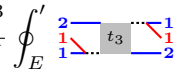

$$= \left(\frac{M_{21}}{2m_r}\right)^{\frac{d}{2}} \oint_E{}' \sum_{\mathbf{p}} t_3(\mathbf{p},\mathbf{p};E)$$
$$\times T_2^2\left(E-\frac{p^2}{2m_{21}}\right)\frac{d}{dE}T_2^{-1}\left(E-\frac{p^2}{2m_{21}}\right).$$

As $E\to-\varepsilon_{\mathrm{b}}$, the 'free' atom-dimer propagator is given by

$$\langle\mathbf{k}|\,\hat{G}_{\mathrm{ad}}(E)\,|\mathbf{k}\rangle \approx \frac{T_2\left(E-\frac{k^2}{2m_{21}}\right)}{g^2Z} \approx \frac{1}{E_{\mathrm{col}}-\frac{k^2}{2m_{21}}}, \tag{B1}$$

where $\pm\mathbf{k}$ are the momenta of the atom and dimer in their center-of-mass frame, the collision energy is given by $E_{\mathrm{col}} = E+\varepsilon_{\mathrm{b}}$ and g^2Z is the residue at T_2's pole given in Eq. (4). In addition, we note that the atom-dimer forward scattering T matrix is given by

$$T_{\mathrm{ad}}(k^2/2m_{21}) = g^2 Z t_3(\mathbf{k},\mathbf{k};k^2/2m_{21}-\varepsilon_{\mathrm{b}}). \tag{B2}$$

Therefore, we obtain

$$B_{21} \overset{\lambda\gg a}{\approx} \left(\frac{M_{21}}{2m_r}\right)^{\frac{d}{2}} \oint_E{}' \sum_{\mathbf{p},\ell} \frac{\xi_\ell T_{\mathrm{ad},\ell}(E_{\mathrm{col}})}{\left(E_{\mathrm{col}}-\frac{p^2}{2m_{21}}\right)^2}$$
$$\approx \left(\frac{M_{21}}{2m_r}\right)^{\frac{d}{2}} e^{\beta\varepsilon_{\mathrm{b}}} \oint_E{}' \sum_{\mathbf{p},\ell} \frac{\xi_\ell T_{\mathrm{ad},\ell}(E)}{\left(E-\frac{p^2}{2m_{21}}\right)^2}, \tag{B3}$$

where we used $\frac{d}{dE}T_2^{-1} \approx g^2Z$ and in the last step, the energy origin is shifted to $-\varepsilon_{\mathrm{b}}$. The full scattering T matrix is given by the partial wave sum $T_{\mathrm{ad}}(s) = \sum_\ell \xi_\ell T_{\mathrm{ad},\ell}(s)$, where we have used the fact that only forward atom-dimer scattering is present in Eq. (B2).

As shown in Section III B, the sum over $\mathbf{p}$ is in fact the sum over the two-body spectrum which is equal to the derivative of the inverse two-body T matrix. That is, we have

$$\sum_{\mathbf{p}}\left(E-\frac{p^2}{2m_{21}}\right)^{-2} \equiv \frac{d}{dE}\sum_\ell \xi_\ell T_{\mathrm{ad},\ell}^{-1}(E). \tag{B4}$$

Following the same analysis, we recast Eq. (B3) in the Beth-Uhlenbeck form

$$B_{21} \overset{\lambda\gg a}{\approx} \left(\frac{M_{21}}{2m_r}\right)^{\frac{d}{2}} e^{\beta\varepsilon_{\mathrm{b}}} \sum_\ell \xi_\ell \int_0^\infty \frac{dk}{\pi} e^{-\beta\frac{k^2}{2m_{21}}} \delta'_{\mathrm{ad},\ell}(k), \tag{B5}$$

which concludes this Appendix.

[1] D. M. Eagles, Phys. Rev. **186**, 456 (1969).

[2] A. J. Leggett, in *Modern Trends in the Theory of Con-*

densed Matter, edited by A. Pekalski and J. Przystawa (Springer-Verlag, Berlin, 1980), p. 14.
[3] C. Comte and P. Nozières, J. Physique **43**, 1069 (1982).
[4] C. A. Regal, M. Greiner, and D. S. Jin, Phys. Rev. Lett. **92**, 040403 (2004).
[5] M. W. Zwierlein, C. A. Stan, C. H. Schunck, S. M. F. Raupach, A. J. Kerman, and W. Ketterle, Phys. Rev. Lett. **92**, 120403 (2004).
[6] C. Chin, M. Bartenstein, A. Altmeyer, S. Riedl, S. Jochim, J. H. Denschlag, and R. Grimm, Science **305**, 1128 (2004).
[7] T. Bourdel, L. Khaykovich, J. Cubizolles, J. Zhang, F. Chevy, M. Teichmann, L. Tarruell, S. J. J. M. F. Kokkelmans, and C. Salomon, Phys. Rev. Lett. **93**, 050401 (2004).
[8] J. Kinast, S. L. Hemmer, M. E. Gehm, A. Turlapov, and J. E. Thomas, Phys. Rev. Lett. **92**, 150402 (2004).
[9] M. Zwierlein, J. Abo-Shaeer, A. Schirotzek, C. Schunck, and W. Ketterle, Nature **435**, 1047 (2005).
[10] P. Nozières and S. Schmitt-Rink, J. Low Temp. Phys. **59**, 195 (1985).
[11] D. E. Sheehy and L. Radzihovsky, Annals of Physics **322**, 1790 (2007).
[12] M. M. Parish, F. M. Marchetti, A. Lamacraft, and B. D. Simons, Nature Phys. **3**, 124 (2007).
[13] S. Pilati and S. Giorgini, Phys. Rev. Lett. **100**, 030401 (2008).
[14] N. Prokof'ev and B. Svistunov, Phys. Rev. B **77**, 020408 (2008).
[15] M. Punk, P. T. Dumitrescu, and W. Zwerger, Phys. Rev. A **80**, 053605 (2009).
[16] C. Mora and F. Chevy, Phys. Rev. A **80**, 033607 (2009).
[17] R. Combescot, S. Giraud, and X. Leyronas, Europhys. Lett. **88**, 60007 (2009).
[18] M. M. Parish, B. Mihaila, E. M. Timmermans, K. B. Blagoev, and P. B. Littlewood, Phys. Rev. B **71**, 064513 (2005).
[19] Y. Sagi, T. E. Drake, R. Paudel, R. Chapurin, and D. S. Jin, arXiv:1409.4743.
[20] E. Beth and G. Uhlenbeck, Physica **IV**, 915 (1937).
[21] A. Pais and G. Uhlenbeck, Physical Review **116**, 250 (1959).
[22] X.-J. Liu, H. Hu, and P. D. Drummond, Phys. Rev. Lett. **102**, 160401 (2009).
[23] X. Leyronas, Phys. Rev. A **84**, 053633 (2011).
[24] D. B. Kaplan and S. Sun, Phys. Rev. Lett. **107**, 030601 (2011).
[25] D. Rakshit, K. M. Daily, and D. Blume, Phys. Rev. A **85**, 033634 (2012).
[26] S. Nascimbène, N. Navon, K. J. Jiang, F. Chevy, and C. Salomon, Nature **463**, 1057 (2010).
[27] M. J. H. Ku, A. T. Sommer, L. W. Cheuk, and M. W. Zwierlein, Science **335**, 563 (2012).
[28] X.-J. Liu, Physics Reports **524**, 37 (2013).
[29] V. Gurarie and L. Radzihovsky, Annals of Physics **322**, 2 (2007).
[30] T.-L. Ho, X. Cui, and W. Li, Phys. Rev. Lett. **108**, 250401 (2012).
[31] R. Dashen, S.-K. Ma, and H. J. Bernstein, Phys. Rev. **187**, 345 (1969).
[32] P. D. Drummond, K. V. Kheruntsyan, and H. He, Phys. Rev. Lett. **81**, 3055 (1998).
[33] D. S. Petrov, C. Salomon, and G. V. Shlyapnikov, Phys. Rev. Lett. **93**, 090404 (2004).
[34] A. Abrikosov, L. Gorkov, and I. Dzyaloshinski, *Methods of quantum field theory in statistical physics* (Dover, New York, N.Y., 1963).
[35] R. K. Pathria, *Statistical Mechanics, Second Edition* (Butterworth-Heinemann, 1996), 2nd ed.
[36] G. V. Skorniakov and K. A. Ter-Martirosian, Sov. Phys. JETP **4**, 648 (1957).
[37] S.-G. Peng, S.-H. Zhao, and K. Jiang, Phys. Rev. A **89**, 013603 (2014).
[38] P. F. Bedaque, H.-W. Hammer, and U. van Kolck, Phys. Rev. C **58**, R641 (1998).
[39] J. Levinsen and D. S. Petrov, Eur. Phys. J. D **65**, 67 (2011).
[40] A. Reiner, Phys. Rev. **151**, 170 (1966).
[41] G. Rupak, Phys. Rev. Lett. **98**, 090403 (2007).
[42] J. Levinsen, T. G. Tiecke, J. T. M. Walraven, and D. S. Petrov, Phys. Rev. Lett. **103**, 153202 (2009).
[43] I. V. Brodsky, M. Y. Kagan, A. V. Klaptsov, R. Combescot, and X. Leyronas, Phys. Rev. A **73**, 032724 (2006).
[44] J. Levinsen and V. Gurarie, Phys. Rev. A **73**, 053607 (2006).
[45] R. K. Bhaduri, W. van Dijk, and M. V. N. Murthy, Phys. Rev. Lett. **108**, 260402 (2012).
[46] H. Hu, X.-J. Liu, P. D. Drummond, and H. Dong, Phys. Rev. Lett. **104**, 240407 (2010).
[47] V. Ngampruetikorn, J. Levinsen, and M. M. Parish, Phys. Rev. Lett. **111**, 265301 (2013).
[48] P. F. Bedaque and G. Rupak, Phys. Rev. B **67**, 174513 (2003).
[49] O. I. Kartavtsev and A. V. Malykh, Journal of Physics B: Atomic, Molecular and Optical Physics **40**, 1429 (2007).
[50] M. Jag, M. Zaccanti, M. Cetina, R. S. Lous, F. Schreck, R. Grimm, D. S. Petrov, and J. Levinsen, Phys. Rev. Lett. **112**, 075302 (2014).
[51] J. Levinsen and M. M. Parish, Phys. Rev. Lett. **110**, 055304 (2013).
[52] D. Blume, Phys. Rev. Lett. **109**, 230404 (2012).
[53] K. M. Daily and D. Blume, Phys. Rev. A **85**, 013609 (2012).
[54] Y. Castin and F. Werner, Canadian Journal of Physics **91**, 382 (2013).
[55] V. N. Efimov, Nucl. Phys. A **210**, 157 (1973).
[56] S. J. J. M. F. Kokkelmans, J. N. Milstein, M. L. Chiofalo, R. Walser, and M. J. Holland, Phys. Rev. A **65**, 053617 (2002).
[57] X.-J. Liu, H. Hu, and P. D. Drummond, Phys. Rev. B **82**, 054524 (2010).
[58] The effective range occurring for zero-range interactions should, of course, be distinguished from a finite range interaction, such as used in Ref. [56].
[59] For the virial expansion in two dimensions, see for instance Refs. [47, 57].
[60] Note that the authors of Ref. [25] recognised that their calculation did not predict the correct fourth virial coefficient.